Early changes in the properties of CA3 engram cells explored with a novel viral tool

Dario Cupolillo[1,2], Noëlle Grosjean[1], Catherine Marneffe[1], Julio Viotti[1], Célia Reynaud[1], Séverine Deforges[1], Mario Carta[1], and Christophe Mulle[1*]

[1]Interdisciplinary Institute for Neuroscience, CNRS UMR 5297, University of Bordeaux, F-33000 Bordeaux, France

[2] current address: Neuroscience and Brain Technologies Department, Fondazione Istituto Italiano di Tecnologia, Genova, Italy

[*]Lead contact; correspondence: christophe.mulle@u-bordeaux.fr

ABSTRACT

Forming new memories after a one-time experience requires initial encoding then consolidation over time. During learning, multimodal information converges onto the hippocampus, activating sparse neuronal assemblies which are thought to form a memory representation through concerted activity and synaptic interconnectivity. In this work, we use a novel tool for fast-labeling of engram neurons (FLEN). FLEN is based on c-Fos activity-dependent transient expression of a destabilized fluorescent marker ZsGreen1 rapidly after one-trial learning. With FLEN, we explore the electrophysiological properties of c-Fos activated CA3 pyramidal neurons a few hours following one-trial learning of an episodic-like memory. In parallel, we employ the Robust Activity Marker (RAM) system, which provides activity-dependent labelling 24 hours following a novel experience. Comparing FLEN+ and RAM+ neurons allows to characterize how the properties of neuronal assemblies evolve during an initial phase of consolidation. Whereas no difference was observed in the excitability of FLEN+ vs. FLEN- neurons, RAM+ neurons were more excitable than RAM- neurons. This suggests that CA3 pyramidal neurons recruited in an engram progressively acquire increased excitability as compared to neurons which were not activated by the one-trial contextual memory task. In contrast, FLEN+ CA3 neurons show an increased number of excitatory inputs. Overall, with the FLEN strategy, we can show that both the intrinsic excitability and the synaptic properties of CA3 pyramidal neurons undergo progressive plastic changes over the first day following a one-trial memory task.

INTRODUCTION

Animal survival depends on the ability to rapidly form new and durable episodic memories of one-time meaningful events which, when recalled, allow to adapt behavior (Tulving, 2002). Contextual memories of ongoing experiences are continuously and rapidly generated in the hippocampus and subsequently stored in an extended cortical network (Eichenbaum, 2000). Computational models of memory point to a crucial role of the hippocampal CA3 region in episodic memory encoding and retrieval (Kesner & Rolls, 2015). Based on its distinctive extensive recurrent architecture (CA3-CA3), CA3 may act as an auto-associative or attractor network, enabling pattern completion during recollection (Kesner & Rolls, 2015; McNaughton, 1987). Indeed, mice with CA3-specific synaptic plasticity impairment (CA3 NR1-KO mice) are unable to encode the novel location of a hidden platform in a delayed matching-to-place version of the Morris water maze (K. Nakazawa et al., 2003) and to retrieve the learned position of a submerged platform when partial cues are presented (K. Nakazawa et al., 2002). In addition to recurrent connections, the main excitatory synaptic drivers of CA3 pyramidal neurons (PNs) are inputs from medial and lateral entorhinal cortex (MEC and LEC) via the perforant pathway (PP), and indirectly from mossy fibers (Mfs) through the dentate gyrus (DG). Mf inputs display 'conditional detonator' properties, enabling individual Mf synapses to trigger postsynaptic firing in response to repetitive firing of presynaptic DG cells (Henze et al., 2002; Marneffe et al., 2024; Rebola et al., 2017; Sachidhanandam et al., 2009; Vandael & Jonas, 2024).

During encoding of novel information, the orchestrated activity patterns of selected neuronal groups distributed throughout the brain, called engrams, represent the initial memory trace (Josselyn & Tonegawa, 2020). Engrams undergo long-lasting synaptic modifications during consolidation and are selectively re-engaged when the memory is retrieved (Bessières et al., 2024; Goto et al., 2021; Josselyn & Tonegawa, 2020; Kitamura et al., 2017; Ryan et al., 2015; Tomé et al., 2024). Experimental manipulation of neuronal engrams in the hippocampus allows selective memory erasure (Han et al., 2009), artificial memory recall (Liu et al., 2012) and creation of a synthetic memory (Vetere et al., 2019), highlighting both their necessity and sufficiency for memory functions.

The investigation of the properties of engram neurons has taken advantage of immediate early genes (IEGs) such as c-Fos, Arc (activity-regulated cytoskeleton-associated protein), or *Npas4* (neuronal PAS domain protein 4) to visualize and label neurons active during a memory task (DeNardo et al., 2019; Kawashima et al., 2013; Reijmers et al., 2007; Sørensen et al., 2016; X. Sun et al., 2020). Generally, IEGs are rapidly and transiently expressed; however different IEGs are triggered by different sets of

extracellular events and possess specific expression kinetics. Temporal control of IEG-based systems is crucial to accurately link engram labeling to specific events that occur in a specific in time.

The activity of engram neurons can be tracked *in vivo* during their maturation from the process of encoding throughout consolidation in behaving mice, by means of functional indicators like GCaMP (Milczarek et al., 2018; Mocle et al., 2024; Tomé et al., 2024). However, *in vivo* Ca^{2+} imaging does not allow to address the synaptic and intrinsic properties of engram neurons. Labeling of engram neurons in order to characterize these properties *ex vivo* over time after an experience has occurred, often relies on labeling techniques using inducible transgenic systems (DeNardo et al., 2019; Reijmers et al., 2007). In several studies using transgenic mouse lines, engram labeling requires 48 hours of doxycycline (Dox) deprivation before a novel experience (Kitamura et al., 2017; Liu et al., 2012; Pignatelli et al., 2019; Ryan et al., 2015), or the use of tamoxifen injection to open a 12-hours time window for engram labeling (DeNardo et al., 2019). Therefore, these systems only offer temporal control over extended time windows, thus increasing the probability of compromising the experience specificity of labeled engram cells. In addition, most of these approaches drive a relatively late labeling, enabling investigation of learning-induced modifications more than 24 hours after a novel experience (e.g RAM system) (X. Sun et al., 2020) or shortly after recall for neurons which have been labeled several days before (Pignatelli et al., 2019), when consolidation processes have already been engaged.

Little has been learned about how neuronal engrams in the hippocampus rapidly (in the time range of hours) adapt their synaptic and physiological properties following encoding of a memory event, and how these properties evolve over time. In this sense, it is unknown whether initial memory storage is enabled by engram cell modifications of intrinsic properties, synaptic plasticity or a combination of them. Here, we tackle these questions using a combination of viral strategies that allow us to identify engram neurons and compare *ex vivo* their properties shortly after learning (3-4 hours), and 24 hours after the experience has occurred (Fig. 1A). To track early engrams, we developed a virally delivered c-Fos-based genetic construct that provides physiological-like rapid expression and fast-decay of the bright fluorescent cytosolic marker ZsGreen1. This novel viral strategy for fast and efficient labeling of engram neurons (FLEN) allows to identify and characterize engram neurons within 3-4 hours following a novel experience, in reference to non-activated neurons. Then, to understand how initial engram cell properties evolve within a 24-hour time scale, we employ the more durable c-Fos-based artificial RAM system (Sørensen et al., 2016) to label neurons and characterize their properties 24 hours after the exposure to a one-trial memory task.

RESULTS

Creation and validation of c-Fos-ZsGreen1-DR for fast-labeling of engram neurons (FLEN).

We generated a genetic cassette for adeno-associated virus-mediated delivery which allows fast labelling of engram neurons (FLEN). This construct includes the full-length, activity-dependent c-Fos promoter which controls the expression of a destabilized variant of the green fluorescent protein ZsGreen1 (Matz et al., 1999) (Fig. 1B). The complete sequence of the c-Fos promoter ensures a physiological-like gene expression of ZsGreen1, which follows c-Fos expression. ZsGreen1 provides a bright whole-cell somatic and dendritic labelling of activated neurons (Fig. 1B). To restrict the labelling time window and minimize labeling unrelated to the designed experience, ZsGreen1 was fused with a destabilizing domain (DR); when fused to EGFP, DR decreases the fluorescence half-time to 2 hours (Li et al., 1998).

To determine the expression kinetics of FLEN in response to neuronal activity, P0 mouse cortical neurons were cultured (cellular density $3x10^5$ cells/well) and then co-infected at DIV3 with AAV9.c-Fos.ZsGreen1-DR (FLEN) and a secondary AAV9.CB7.mCherry, which constitutively expresses mCherry in infected neurons (Fig. 1B-C). Neurons were cultured until DIV11 in regular neurobasal medium, before switching to an activating medium containing 4-aminopyridine (4-AP, 100 µM) and bicuculline (Bic, 10 µM) for 30 minutes. The drugs were then washed out, and tetrodotoxin (TTX, 0.5 µM) was added to block further neuronal activity until cells were fixed (Fig. 1C). The percentage of activated neurons (ZsGreen+, further named FLEN+ neurons) over the total number of transduced neurons (mCherry+ neurons) was calculated at different time points within a 6-hour period after pharmacological stimulation. Only a limited number of FLEN+ neurons could be found in unstimulated conditions (5.4 ± 0.5 FLEN+/FLEN-, n=3 plates) (Fig. 1D-E). The activating medium triggered ZsGreen1 expression in neurons as early as 2 hours, reaching a 3-fold peak within 3 hours (1 hour: 6.7 ± 1.0, n=3; 2 hours: 13.2 ± 5.0, n=3; 3 hours: 15.7 ± 2.2, n=5) (Fig. 1D-E). The number of FLEN+ neurons decreased after the peak, decaying to pre-stimulation-like levels within 6 hours (4.5 hours: 12.0 ± 3.9, n=4; 6 hours: 5.0 ± 1.1, n=4) (Fig. 1D-E). Thus, FLEN showed a rapid induction (2-3 hours) and a fast decay (within 6 hours) of ZsGreen1-DR fluorescence (one-way ANOVA, p=0.04).

FLEN captures early neuronal activity following CFC

We next investigated the time course of FLEN expression *in vivo* in wild-type mice in response to exposure to a salient novel experience. We virally targeted bilaterally dorsal CA3 in adult mice (2–3-month-old) co-injecting AAV9.c-Fos.ZsGreen1-DR and the infection control AAV9.CB7.mCherry (Fig. 2A). Then, mice were subjected to contextual fear conditioning (CFC), a hippocampal-dependent one-trial memory task. During this task, mice learned to associate the delivery of 3 mild foot-shocks (0.4 pA, 2 seconds) with a specific

environment (Fig. 2B). We found that CFC, a one-trial experience, can generate a strong context-specific fear memory, as mice responded by freezing when re-exposed to the conditioning environment 1 hour after training (HC: 14.7% ± 2.3%, 1-hour post-CFC: 47.4% ± 7.9%, n=7; unpaired t-test, p=0. 0018), a response that outlasted 24 hours after training, but was not triggered in an unfamiliar novel environment, nor when they were left undisturbed in their home cage (HC) (HC: 18.7% ± 3.5%, 24 hours post-CFC: 61.5% ± 7.5%, neutral: 14.3% ± 4.5%, n=8; one-way ANOVA, Tukey's post-hoc test HC : 1 hour post-CFC p =0.00004, HC : Neutral p=0 .84116, Neutral :1 hour post-CFC p=0.00001) (Fig. 2B).

The percentage of FLEN+ CA3 neurons (i. e. that display FLEN+/mCherry+ labeling, Fig. 2C) among the overall population of infected neurons (FLEN-, i. e. that display mCherry+ labeling) was quantified 1.5, 3, 4.5, 6 and 12 hours following CFC and compared to that of untrained mice. Consistent with previous studies (Sørensen et al., 2016; Weng et al., 2018), less than 2% of infected CA3 neurons were reported to be labeled in the absence of a novel experience (Fig. 2D-E, HC, 0.84% ± 0.29% FLEN+/mCherry+, n=6). One-trial CFC conditioning generated an engram, as indicated by an increase in FLEN+ neurons in CA3 in the following hours (Fig 2D-E). Specifically, CA3 displayed 1.11% ± 0.42% FLEN+ neurons 1.5 hours after CFC (n=5), which increased to 3.11% ± 0.74% 3 hours post-CFC (n=4) and 2.31 ± 0.44% at 4.5 hours post-CFC (n=7). The fraction of active cells returned to basal-like levels at 6 hours (1.86 ± 0.16% FLEN+/ mCherry+, n=5) and further decreased 12 hours post-CFC (0.73% ± 0.32% FLEN+/ mCherry+, n=4) (Fig. 2D-E). Overall, the emergence of FLEN assembly peaks 3 hours following CFC and significantly decreases 12 hours later (one-way ANOVA p=0.003, *post hoc* Tukey's multiple comparisons test: HC vs. 3 h p=0.008, 1.5 h vs. 3 h p=0.04, 3h vs. 12h p=0.01), faithfully mimicking the progression and transient nature of native c-Fos expression (Holtmaat & Caroni, 2016).

We sought to probe CA3 engram formation 3 hours after different behavioral situations, namely context-only (CO) and immediate-shock (IS) conditions, which offer the possibility for spatial exploration only and no spatial exploration at all, respectively (Fig. S1A). In CO conditions, mice were allowed to freely explore a novel cue-enriched arena. Comparably to other exploratory tasks, we found an increase in the number of FLEN+ CA3 PNs 3 hours following CO (3.50 ± 1.18 % FLEN+/FLEN-, n=5) compared to control HC mice (Kruskal-Wallis non-parametric test, p=0.03; Dunn *post hoc* multiple comparisons test, p=0.02) (Fig. S2B). In the IS test, a 6-second-long foot-shock was delivered 2 seconds after the mouse was placed in the conditioning cage, preventing sensorial sampling of the novel context (Fig. S1A). In contrast, the IS test did not induce a significant increase in the number of FLEN+ in CA3 PNs as compared to HC (1.84 ± 0.77 %

150 FLEN+/FLEN-, n=4; Dunn *post hoc* multiple comparisons test, HC: IS, p=0.51) and to context-only (CO: IS,
151 p=0.88, n=4), possibly because of minimal spatial exploration.

152 Because of the reported functional heterogeneity of CA3 PNs in relation to memory encoding and recall,
153 which is directly related to their position within the proximodistal axis of CA3 (Nakamura et al., 2013; Y.
154 Nakazawa et al., 2016; Q. Sun et al., 2017), we analyzed the spatial distribution of FLEN+ PNs within CA3
155 pyramidal layer along the proximodistal and superficial-to-deep axis of CA3, following one-trial CFC (Fig.
156 2F and Fig. S2). We found a clear skewedness in the location of FLEN+ neurons along the proximodistal
157 axis toward CA3a at all time points following CFC and following CO compared to HC (Kolmogorov-Smirnov
158 test: HC vs. 1.5 h post-CFC, p<0.001; HC vs. 3 h post-CFC, p<0.001; HC vs. 4.5 h post-CFC, p<0.001; HC vs.
159 6 h post-CFC, p<0.001: HC vs. 12 h post-CFC, p<0.001; HC vs. CO, p<0.001: HC vs. IS, p<0.001) whilst they
160 appeared to be more evenly distributed along the superficial-deep axis (Kolmogorov-Smirnov test: HC vs.
161 1.5 h post-CFC, p=0.013: HC vs. 3 h post-CFC, p<0.001; HC vs. 4.5 h post-CFC, p<0.001; HC vs. 6h post-CFC,
162 p<0.001; HC vs. 12 h post-CFC, p=0.61; HC vs. CO, p<0.001: HC vs. IS, p=0.02) (Fig. 2F and Fig. S2). Overall,
163 these data indicate that the FLEN labeling strategy faithfully identifies neurons activated during a one-trial
164 exposure to a novel context and allows to characterize the morpho-functional properties of CA3 engram
165 neurons shortly (< 6 hours) following the experience.

166 In parallel, we confirmed that the RAM system (Sørensen et al., 2016) is a powerful tool to tag neurons
167 selectively activated by CFC in a temporally controlled manner (Fig. S3A) (Sørensen et al., 2016; Weng et
168 al., 2018). To identify RAM+ neurons, we stereotaxically injected AAV9.RAM.2dtTA::TRE.EGFP and
169 AAV9.CB7.mCherry to label dorsal CA3 in wild-type mice (Fig. S3A). Mice were fed with doxycycline pellets
170 starting one day before injection and then switched to a regular food diet for 48 hours before CFC (Fig.
171 S3A). As reported, we found that the number of RAM+ neurons was notably higher 24 hours after CFC
172 with respect to HC conditions (% RAM+ vs. mCherry+ neurons, HC: 1.13 ± 0.18%, n=5; CFC: 3.54 ± 0.77%,
173 n=5; Welch's t-test p=0.03) (Fig. S3B-C), although not to the same extend as in previous reports (Sørensen
174 et al., 2016). The ratio of FLEN+ neurons 3 hours after CFC over HC (approximately 3:1) closely resembles
175 that of RAM+ neurons 24 hours after CFC (approximately 3:1)

176 **CA3 engram neurons evolve from low to higher firing frequency over 24 hours**

177 To understand if rapid memory acquisition and early consolidation is supported by specific changes in
178 electrophysiological intrinsic properties, we performed whole-cell patch-clamp recordings of CA3 PNs
179 (mainly in CA3b) in acute hippocampal slices of young adult mice injected with either FLEN or RAM,
180 respectively (Fig. 3A). AAV9.c-Fos.ZsGreen1-DR or AAV9.RAM.2dtTA::TRE.EGFP viral constructs were

181 injected bilaterally in dorsal CA3, together with AAV9.CB7.mCherry (Fig. 3A). After CFC, mice were
182 returned to their home cage for 3 hours (FLEN) or 24 hours (RAM), to yield peak expression of ZsGreen1-
183 DR or EGFP and then sacrificed to collect parasagittal slices (Fig. 3A). Activity-dependent FLEN+ neurons
184 remained detectable in acute slices, enabling specific targeting of engram CA3 PNs neurons for
185 approximately 4 to 5 hours after slicing. Engram neurons (FLEN+ or RAM+) were compared to their
186 respective neighboring non-engram neurons (FLEN- or RAM-) (Fig. 3A).

187 We first investigated the intrinsic physiological properties of FLEN+ and RAM+ CA3 PNs. Indeed, the
188 probability for a neuron to be recruited in a memory engram is thought to depend on its inherent
189 excitability level at the time of learning (see Josselyn & Tonegawa, 2020 for review). We assessed input
190 resistance (R_i) by injecting a series of hyper- and depolarizing current pulses with the membrane potential
191 held at -70 mV (Fig. 3B). R_i did not change significantly between FLEN+ and FLEN- neurons (FLEN+: 253 ±
192 35 MΩ, n=19; FLEN-: 210 ± 19 MΩ, n=30; non-parametric Mann-Whitney U test, p-value=0.57) and was
193 similar to RAM+ and RAM- neurons which were also no different between them (RAM+: 323.7 ± 14.1 MΩ,
194 n=21; RAM-: 396.1 ± 15.2 MΩ, n=30, parametric t-test, p=0.68) (Fig.3B). Further depolarizing steps of
195 current were injected until an action potential was fired. Action potential properties such as threshold,
196 amplitude, width, upstroke and downstroke were not statistically different between FLEN+ and FLEN-
197 neurons and between RAM+ and RAM- neurons (Fig. S4B, C; Table 1). To study the action potential firing
198 pattern, we injected 1 s-long pulses of current just above rheobase (200 pA) (Fig. 3C). Overall, the firing
199 frequency was not different in the FLEN groups (FLEN+: 2.64 ± 0.65 Hz, n=9; FLEN-: 3.59 ± 0.62 Hz, n=19;
200 Mann-Whitney U test, p=0.51) (Fig. 3C). More than half of the total number of action potentials occurred
201 within the first 100 ms for all CA3 PNs, showing a consistent discharge pattern across both FLEN+ and
202 FLEN- cells (Kolmogorov-Smirnov test, p-value=1.0) (Fig. 3D). In contrast to FLEN+ CA3 PNs, RAM+ CA3
203 PNs showed a prolonged spiking activity which outlasted the first 100 ms (Fig. 3D). This is reflected by an
204 overall increased number of APs (RAM+: 20.9 ± 1.5 Hz, n=13; RAM-: 7.1 ± 0.6 Hz, n= 15; Mann-Whitney U
205 Test p=0.04) (Fig. 3C). CA3 PNs have been reported to have a distinctive burst-like firing pattern relying
206 on the generation of dendritic Ca^{2+} spikes (Ding et al., 2020; Raus Balind et al., 2019). We defined bursts
207 as a firing pattern where two or more spikes occur within a 50 ms interval (Zucca et al., 2017). Bursts were
208 triggered by rheobase current pulses in 7 out of 19 FLEN- CA3 PNs (36.8 ± 12.9 %, with an average of 2.33
209 ± 0.33 spikes per burst), but only 1 out of 9 FLEN+ neurons displayed bursting behavior (11.1 ± 12.9 %,
210 with 3.86 average spikes per burst). Bursts were induced in 6 out of 15 RAM- neurons (40.0 ±4.6 %, with
211 an average of 2.13 ± 0.07 spikes per burst). However, contrarily to FLEN+ neurons, 30.8 ± 4.6 % (4 out of
212 13 CA3-PN RAM+ neurons with an average spike/burst of 2.10 ± 0.10), indicating a 2.7-fold increase in the

213 propensity of CA3 engram neurons to display bursting behavior over 24 hours after CFC (Fig 3D).
214 Altogether, these results show that early after encoding, FLEN+ CA3 PNs do not show differences in
215 excitability or patterns of bursting activity as compared to control neurons. However, after 24 hours, CA3
216 engram cells display an increase in excitability and in bursting behavior without changes in R_i.

217 **Synaptic properties of FLEN+ neurons**

218 To assess overall excitatory synaptic strength and overall number of active synaptic connections, we
219 recorded spontaneous excitatory post-synaptic currents (sEPSCs) in FLEN+ CA3 PNs while blocking $GABA_A$-
220 dependent inhibitory currents (Bicuculline, 10 µM). The average amplitude of sEPSCs was not different
221 between FLEN+ and FLEN- CA3 PNs (FLEN+: 29.7 ± 5.3 pA, n=9; FLEN-: 32.2 ± 3.7 pA, n=9; Kolmogorov-
222 Smirnov test, p = 0.99), whereas their frequency was increased (Inter-event interval (IEI), FLEN+: 788 ±
223 152 ms, n=10; FLEN-: 930 ± 91 ms, n=10; Kolmogorov-Smirnov test, p < 0.005) (Fig. 4A). Similarly, 24 hours
224 after a novel experience, the average amplitude of sEPSCs was similar between RAM+ and RAM- CA3 PNs
225 (RAM+: 26.22 ± 2.46 pA, n=14; RAM-: 21.31 ± 2.72 pA, n=14, Kolmogorov-Smirnov test, p=0.99) (Fig. 4A),
226 but their frequency was significantly increased in RAM+ CA3 PNs (RAM+: 645 ± 88 ms, n=17; RAM -: 1342
227 ± 207 ms, n=17; Kolmogorov-Smirnov test, p < 0.05) (Fig. 4A).

228 Then, to investigate excitatory synaptic strength and release probability independent of network activity,
229 we measured miniature EPSCs (mEPSCs) by further adding TTX (0.5 µM). The average amplitude was
230 similar between FLEN+ and FLEN- neurons (FLEN+: 20.5 ± 2.5 pA, n=9; FLEN-: 18.7 ± 1.6 pA, n=14;
231 Kolmogorov-Smirnov test, p = 0.99), whereas we observed a higher frequency of mEPSCs in FLEN+ neurons
232 as compared to control neurons (IEI, FLEN+: 1722 ± 242 ms, n=9; FLEN-: 1228 ± 186 ms, n=14; Kolmogorov-
233 Smirnov test, p < 0.0005) (Fig. 4B). Comparably, we found a higher frequency of mEPSCs in RAM+ neurons
234 as compared to RAM- CA3 PNs (RAM+: 782 ± 91 ms, n=14; RAM-: 1244 ± 247 ms, n=13; Kolmogorov-
235 Smirnov test, p<0.005), with unchanged amplitude (RAM+: 29.6 ± 4.8 pA, n=14: RAM-: 24.7 ± 4.2 pA, n=13;
236 Kolmogorov-Smirnov test, p=0.99) (Fig. 4B). Thus, neurons recruited in an engram appear to show
237 increased excitatory drive after a few hours that persist after 24 hours, which may be linked to a higher
238 number of synaptic contacts.

239 Previous reports indicate that CA3 PNs activated during by contextual learning and identified 24 hours
240 later by RAM had strengthened mossy fiber inputs (Weng et al., 2018). The existence of mEPSCs with
241 larger amplitudes may be related to synaptic plasticity in a subset of synapses, or theoretically to an
242 increased participation of Mf-driven mEPSCs (Henze et al., 2002). We thus calculated the proportion
243 miniature excitatory events with an amplitude greater than 40 pA. During spontaneous activity recording,

244 we found no difference in the fraction of putative Mf-driven inputs between FLEN+ and FLEN- PNs (FLEN+:
245 0.09 ± 0.03 %, n= 9; FLEN-: 0.06 ± 0.02%, n=14; Mann-Whitney U Test p=0.33) and between RAM+ and
246 RAM- PNs 24 hours after learning (RAM+: 0.25 ± 0.08 %, n= 14; RAM-: 0.18 ± 0.07 %, n=13; Mann Whitney
247 U test, p=0.42) (Fig. 4B, inset). This later finding contrasts with earlier finding (Weng et al., 2018), which
248 found a selective strengthening of Mf inputs onto the ensemble of CA3 neurons >24hours after activation
249 by CFC. At variance with our analysis, this later study uses a mGluR2/3 agonist, LY354740, which inhibits
250 evoked Mf-CA3 synaptic transmission (Kamiya & Ozawa, 1999).

251 Inhibitory neurons are important in controlling spike generation of CA3 PNs, shaping network activity and
252 participation in neuronal assembly formation (Holtmaat & Caroni, 2016). We therefore probed miniature
253 inhibitory post-synaptic currents (mIPSCs), comparing FLEN+ vs. FLEN- neurons and RAM+ vs. RAM-
254 neurons, in the presence of NBQX (20 µM), D-AP5 (50 µM) and TTX (0.5 µM). We found that mIPSCs were
255 statistically more frequent (FLEN+: 340.1 ± 4.0 ms, n=4; FLEN-: 511.0 ± 40.5 ms, n=14; Kolmogorov-
256 Smirnov test, p < 0.005), but their amplitude was on average comparable in FLEN+ vs. FLEN- neurons
257 (FLEN+: 35.1 ± 2.3 pA, n=4; FLEN+: 31.7 ± 2.2 pA, n=14; Kolmogorov-Smirnov test, p = 0.99) (Fig 5A). At 24
258 hours after learning, RAM+ neurons showed an increase in the frequency of mIPSC (IEI 330.5 ± 51.9 ms,
259 n=6) compared to RAM- neurons (IEI 437.1 ± 47.1 ms, n=11; Kolmogorov-Smirnov test, p < 0.005), but no
260 difference in their amplitude (RAM+: 22.7 ±1. 8 pA, n=11; RAM-: 26.5 ± 5.2, n=6; Kolmogorov-Smirnov
261 test, p=0.89) (Fig. 5A). The frequency of all excitatory and inhibitory inputs was elevated after CFC, both
262 after 3 hours and after 24 hours, but not their amplitude.

263 **Mf-CA3 synapses and feedforward inhibition in FLEN+ neurons**

264 Mf-CA3 connections between the DG and CA3 pyramidal cells provide powerful inputs via 'giant' Mf
265 boutons to CA3 PCs, which are thought to assist CA3 in the encoding of memory (Marneffe et al., 2024;
266 Vandael & Jonas, 2024). We recorded EPSCs evoked by minimal stimulation of Mfs (Marchal & Mulle,
267 2004) in FLEN+ and FLEN- CA3 PNs using an extracellular electrode placed within the DG hilus to stimulate
268 the Mf axonal bundle (fig. 6A). Low-frequency stimulation (0.1 Hz) evoked EPSCs of variable amplitude
269 that, on average, did not differ between FLEN+ (81.7 ± 17.5 pA, n=5) and FLEN- neurons (80.8 ± 13.5 pA,
270 n=8; Welch's t-test p = 0.97) (Fig. 6B). Increasing stimulation frequency to 1 Hz induced short-term
271 presynaptic frequency facilitation, causing an approximatively 3-fold increase in evoked current amplitude
272 in both FLEN+ (258.3 ± 49.5 pA, n=5) and FLEN- neurons (238.2 ± 39.0 pA, n=8; Welch's t-test p = 0.76)
273 (Fig. 6B). The EPSC facilitation ratio (1Hz vs. 0.1 Hz) was not different between FLEN+ and FLEN- neurons
274 (FLEN+: 3.28 ± 0.40, n=5; FLEN-: 3.28 ± 0.57, n=8; Welch's t-test p = 0.99) (Fig. 6B).

275 One-trial memory tasks reversibly induce a robust and rapid (within hours) increase in the number of
276 filopodia emanating from Mf synaptic terminals which contact GABAergic interneurons (Ruediger et al.,
277 2011), lending support to the hypothesis of an increase in feedforward inhibition in most CA3 PNs.
278 Because of the rapid time course with which structural plasticity occurs at Mf-CA3 synapses following one-
279 trial memory task, we took advantage of FLEN in order to explore a functional counterpart to structural
280 plasticity, and to address whether the change in feedforward inhibition was differentially affected in
281 FLEN+ vs. FLEN- CA3 PNs. We recorded excitatory and inhibitory synaptic currents in CA3 PNs while
282 stimulating Mfs (Fig. 6A). To calculate the excitatory to inhibitory (E/I) ratio at these synapses, we first
283 recorded evoked EPSCs by holding cells at the experimentally determined $GABA_A$ reversal potential (E_{Cl1-}
284 =-70 mV), and then at the reversal potential for cations (E_{Na1+} = +5 mV) (Fig. 6C) (Torborg et al., 2010). We
285 measured the peak amplitude of evoked EPSCs and IPSCs at a stimulation rate of 0.1 Hz to prevent
286 frequency facilitation (Fig. 6C). We found that the EPSC/IPSC ratio was higher in FLEN+ vs FLEN- cells,
287 although this not significantly different (FLEN+: 3.48 ± 0.96, n=5; FLEN-: 2.20 ± 0.42, n=8; Welch's t-test, p
288 = 0.27) (Fig. 6C). These data do not support the notion that shortly after one-trial learning, there is an
289 increase in feedforward inhibition at Mf-CA3 synapses.

290 **DISCUSSION**

291 In the past decade, the search for engrams and the characterization of engram cells has largely benefited
292 from new gene targeting approaches to label the cells and to control their reactivation (Josselyn &
293 Tonegawa, 2020). The primary goal of our work was to test the hypothesis that the functional properties
294 of hippocampal cells activated during a one-trial contextual memory task were distinct from surrounding
295 ones shortly (3-6 hours) after encoding and were subject to progressive plastic changes which could be
296 linked to a first phase of memory consolidation.

297 Most techniques currently employed to study the properties of engram cells *ex vivo*, combine promoter
298 expression based on IEGs, intersectional transgenic strategies, optogenetics and pharmacogenetics with
299 behavioral paradigms (Denny et al., 2014; Pignatelli et al., 2019; X. Sun et al., 2020; Tonegawa et al., 2015).
300 A major caveat for using activity-dependent promoter/enhancers is the background basal expression
301 which can result in the labeling of neurons unrelated to the triggering behavioral event. To limit this,
302 fluorescent marker and/or actuator expression can be temporally controlled by directly coupling IEG
303 promoters, such as c-Fos or synthetic promoters (RAM), to inducible systems such as the doxycycline (Dox)
304 or the tamoxifen (TAM) systems 11/28/2024 11:00:00 PMWith these approaches, the physiological
305 properties of engram vs. non-engram cells has been examined by *ex vivo* patch-clamp recordings 24 hours

306 to several days after the initial contextual memory task (Pignatelli et al., 2019; Sørensen et al., 2016; Weng
307 et al., 2018; Yap et al., 2021).

308 We thus developed a viral strategy for transient neuronal expression of a fluorescent protein (FLEN)
309 following the exposure of mice to a novel context making use of the full-length c-Fos promoter and of the
310 brightly fluorescent ZsGreen1 protein engineered to be quickly destabilized. The time course of expression
311 of ZsGreen1 in FLEN labeled neurons peaked at 3 hours both after pharmacological activation in cultured
312 neurons and *in vivo* after a 5-minute exposure to a novel context. Neuron labeling persisted for a few
313 hours, enabling *ex vivo* electrophysiological characterization of neurons thought to be involved in the
314 initial encoding of contextual memory. As with all techniques based on IEG promoters, a small percentage
315 of AAV-transduced neurons showed ZsGreen1 fluorescence under control conditions (HC or no activation
316 of cultured neurons). However, following CFC, the number of FLEN labeled neurons increased by a factor
317 of 3.12. The bright fluorescence of ZsGreen1 enabled the electrophysiological characterization of FLEN+
318 neurons, the majority of which (>60%) were activated in relation to the CFC memory task.

319 We have used FLEN to label neurons in CA3, which is involved in the rapid encoding of new spatial and
320 contextual information (Kesner and Rolls, 2015). One of the key features of CA3 is the presence of
321 recurrent excitatory connections which are subject to NMDA-dependent synaptic plasticity (Rebola et al.,
322 2017), and this appears essential for memory of a one-trial experience (K. Nakazawa et al., 2003). It has
323 been proposed that the excitability state of neurons may contribute to memory formation (Zhang &
324 Linden, 2003). We first examined whether FLEN+ neurons showed distinctive intrinsic excitability
325 properties. We observed no difference in the membrane potential, input resistance, threshold or bursting
326 activity between FLEN+ and FLEN- neurons in slices prepared 3 hours following CFC. This suggests that the
327 subpopulation of CA3 PNs engaged in a one-trial learning task are not initially more excitable than the
328 general population of neurons, hence are not predetermined by their excitability state. Alternatively,
329 engram neurons may be transiently more excitable, at the time of encoding, and lose this property within
330 a few hours. In apparent contrast with our finding that FLEN+ CA3 PNs did not show increased excitability,
331 a simple associative memory task, trace eye-blink conditioning, appears to increase the excitability of a
332 large fraction (more than half) of CA3 neurons starting at 1 hour and decreasing after several days
333 (Thompson et al., 1996). Beyond the difference in the task and in the species, these contrasting results
334 may be explained by an overall increased activity of CA1 neurons related to the learning task (Cai et al.,
335 2016; Moyer et al., 1996), however not specific to engram neurons. This does not preclude however the
336 possibility that relative neuronal excitability immediately before training could contribute to the selection

337 of neurons to an engram as proposed in the amygdala (Yiu et al., 2014) and the hippocampus (Mocle et
338 al., 2024). However, in our hands, a one-trial memory task does not per se trigger a selective increase in
339 the excitability of engram neurons 3 hours after CFC as compared to the general population of CA3
340 neurons. In the DG, recall of a previously stored contextual memory (48 hours before), hence reactivation
341 of engram neurons, rapidly increased the excitability of these engram neurons (within 1 hour) with respect
342 to engram neurons which were not subject to reactivation in a separate group of mice (Pignatelli et al.,
343 2019). A learning-related task may however induce plasticity of intrinsic excitability of engram neurons on
344 a longer time scale. We thus compared the intrinsic excitability of FLEN+ neurons to those labeled more
345 than 24 hours after CFC by using the previously described RAM (Sørensen et al., 2016). We found that
346 RAM+ neurons showed prolonged spike firing in response to a depolarizing pulse of current, hence
347 decreased accommodation in comparison with non-labeled neurons. Considering that the set of neurons
348 labeled by these two strategies may be of the same set, based on the expression of a fluorescent marker
349 under the control of the c-Fos promoter, our data strongly suggest that engram neurons in CA3
350 progressively increase excitability as compared to neurons which were not activated by the one-trial
351 contextual memory task. The acquisition of increased excitability 24 hours after one-trial memory
352 encoding suggests that intrinsic excitability is a key feature of an early consolidation of memory, which
353 may even be strengthened upon reactivation of memory (Pignatelli et al., 2019). It would be interesting
354 to assess whether increased intrinsic excitability persists throughout further consolidation of memory.

355 Increased neuronal activity in engram neurons at the time of encoding may result from more efficient or
356 more synchronous excitatory synaptic inputs to these neurons. Here we observed that FLEN+ neurons
357 (hence characterized >3 hours after initial encoding) showed an increased excitatory drive, which may be
358 explained by a higher number of synaptic contacts. We cannot discriminate whether the increased
359 number of synaptic inputs preexists to the formation of the engram, or whether it is a plastic mechanism
360 taking place shortly following the contextual memory. The time course of appearance of additional
361 synapses, by unmuting of silent synapses following contextual memory acquisition, is compatible with
362 experimentally induced functional and structural synaptic plasticity (Holtmaat & Caroni, 2016). On the
363 other hand, if FLEN+ neurons showed higher synaptic inputs at the time of memory encoding, this would
364 increase the chance that these neurons show increased excitation (c-Fos activation) hence participate in
365 the engram. The amplitude of mEPSCs in FLEN+ neurons does not appear to increase on average in
366 comparison with FLEN- CA3 PNs. This finding may not favor the possibility that LTP-like synaptic plasticity
367 occurs early during the process of memory formation. In this event, NMDA-dependent forms of synaptic
368 plasticity are more likely to occur later on during the early phase of consolidation of the memory trace

369 (Humeau & Choquet, 2019). Interestingly, we observed a comparable increase in the frequency of sEPSCs
370 and mEPSCs in RAM+ CA3 neurons 24 hours after CFC, as previously reported (Weng et al., 2018), without
371 any change in the amplitude. Using a pharmacological agent which selectively inhibits Mf-CA3
372 transmission, it was hypothesized that the increased mEPSC frequency is mainly due to more active Mf-
373 CA3 synapses (Weng et al., 2018). However, if this was the case, we would also expect an increase in the
374 amplitude of mEPSCs as well as an increase in the fraction of mEPSCs larger than 45 pA. In addition, we
375 did not find evidence for an increase in Mf-CA3-evoked EPSCs (see below). Overall, our data indicates that
376 CA3 engram neurons characterized a few hours after the one-trial memory task show a higher level of
377 excitatory synaptic inputs, and this feature seems to extend to 24 hours. We found no evidence for
378 increased amplitude of EPSCs in FLEN+ or RAM+ CA3 PNs which could have been indicative of postsynaptic
379 plasticity through an increased number of synaptic AMPA receptors (Humeau & Choquet, 2019; Takeuchi
380 et al., 2014). One reason may be that synaptic plasticity only occurs in a subset of synaptic contacts, and
381 the recording of mEPSCs is not resolutive enough to capture these modifications

382 Local inhibition controls the spiking of CA3 PNs, hence their capacity to be engaged in an active ensemble
383 of neurons at the time of contextual memory encoding. In CA1, there is a fine control of inhibition upon
384 novel environment exploration (Yap et al., 2021) or fear learning (Lovett-Barron et al., 2014). We found
385 an increase in the frequency of mIPSCs after CFC in engram CA3 neurons, both after 3 hours and after 24
386 hours. This suggests that the elevation of mEPSCs in the engram neurons is counterbalanced by increased
387 inhibition, although this would need to be generally tested in conditions of hippocampal circuit activity *in*
388 *vivo*. We have also provided information on the process of Mf-driven feedforward inhibition in CA3
389 following one-trial memory encoding. Mf-CA3 synapses have been proposed to play a major role in
390 assisting CA3 in the encoding of memory (Kesner & Rolls, 2015). For these reasons, it is important to
391 directly characterize the properties of Mf-CA3 synapses impinging on CA3 engram neurons. We observed
392 no difference in the amplitude and short-term plasticity of Mf-CA3 EPSCs evoked in FLEN+ CA3 neurons
393 vs. FLEN- neurons. It has been proposed that 24 hours after CFC, the increased amplitude of mEPSCs in
394 RAM+ neurons can be attributed to modifications of Mf-CA3 synapses (Weng et al., 2018), which may
395 suggest progressive plasticity of these inputs. There is abundant evidence that the structural properties
396 of Mf-CA3 synapses are modified by experience (Ruediger et al., 2011)(Galimberti et al., 2006; Maruo et
397 al., 2016). Feedforward inhibition combines with short-term plasticity of Mf-CA3 synapses to define the
398 physiological conditions for efficient spike transfer between the DG and CA3 (Marneffe et al., 2024;
399 Vandael & Jonas, 2024; Zucca et al., 2017). CFC induces a robust and global increase in the number of
400 filopodia emanating from the giant Mf terminals, which peaks between 1 and 5 hours after the one-trial

401 memory task and is related to the precision of memory and the size of engrams (Ruediger et al., 2011).
402 Because filopodia contact GABAergic interneurons, this structural plasticity has been proposed to increase
403 feedforward inhibition, albeit this has not yet been demonstrated. Here we compared the
404 excitation/inhibition ratio of Mf-evoked synaptic responses between FLEN+ and FLEN- neurons. We did
405 not observe a significant increase of feedforward inhibition onto CA3 engrams, as may be expected from
406 an increase number of filopodia, but we rather observed a tendency towards less feedforward inhibition.
407 This leads us to speculate that shortly following contextual memory formation, Mf-driven feedforward
408 inhibition is increased in the general population of neurons but not in Mf inputs onto engram neurons,
409 thus allowing for a comparatively stronger input from the DG to the engram neurons. It will be interesting
410 to test whether this increased signal to noise ratio is maintained 24 hours after contextual memory
411 encoding, given that the number of filopodia per Mf bouton has returned to basal level (Ruediger et al.,
412 2011).

413 In conclusion, we used a viral tool allowing for the identification of neurons involved in a behavioral task
414 within 3 hours, as a complement to the transgenic mouse strategies and viral vectors which have been
415 used to assess changes in engram neuron properties in the time range of days. Although it is not possible
416 to fully assess the electrophysiological properties of engram neurons at the time of the encoding, this
417 work shows that the engram neurons are not different in their intrinsic membrane properties shortly after
418 encoding. This set of properties may however follow delayed (progressive) plastic changes which are
419 evident 24 hours after initial encoding. Overall, we propose that engram neurons do not show higher
420 excitability preexisting to the selection of neurons to the engram during the memory encoding task. Hence
421 the increased activation state of the FLEN+ neurons at the time of encoding may rather relate to a higher
422 number of active synaptic inputs providing more efficient excitation. Interestingly, although more work is
423 needed to confirm this tendency, increased excitation may also be linked to decreased Mf-driven
424 feedforward inhibition, thus favoring spike transfer from the DG to CA3 at the time or shortly after
425 memory encoding. The FLEN viral tool will be useful to assess how the properties of neurons in brain
426 regions are involved in the contextual memory encoding process, including the entorhinal cortex and the
427 DG.

428 **METHODS**

429 **Animals.** C57Bl6j female mice were obtained from Janvier and cared according to the regulations of the
430 University of Bordeaux/CNRS Animal Care and Use Committee. Animals were housed with their
431 littermates with ad libitum access to food and water. Cages were kept in a temperature-regulated room
432 on a 12 h light/dark cycle. Prior to any behavioral test, all mice were single housed for 4-5 days and then
433 handled for at least 3 consecutive days. Mice injected with the RAM system were kept on a doxycycline
434 diet (4 mg/Kg) starting 1 day before the viral injection.

435 **Viral vectors.** Adeno-associated virus (AAV) serotype 2/9 (capsid is AAV9 and the machinery and ITR are
436 AAV2) vectors containing our custom-made c-Fos.ZsGreen1-DR (titer 4.00E13) were generated in our lab,
437 whereas AAV2/9 vectors containing the RAM system (titer 3.39E13) were purchased from AddGene. Each
438 vector was mixed with an infection marker virus AAV9.CB7.mCherry (titer 1.50E13) and diluted 1:10 for
439 co-injection.

440 **Cell Culture.** P0 mouse cortical neurons were plated (300000 cells/well) and allowed to grow on glia cells.
441 At DIV3 cells were infected with the viral mix of AAV9.c-Fos.ZsGreen1-DR and AAV9.CB7.mCherry. At
442 DIV14, neurons were switched to an activating medium containing 4-AP (100 µM) and Bicuculline (10 µM)
443 for 30 minutes. Then this activating medium was washed and tetrodotoxin was added (0.5 µM) to prevent
444 action potential firing and stop neuronal activation. Neurons were then fixed using 0.4%
445 paraformaldehyde (PFA) in 0.1 mM PBS at the different intervals following pharmacological activation.

446 **Stereotaxic injection.** 2-month-old C57Bl6j mice were bilaterally injected with either AAV9.c-
447 Fos.ZsGreen1-DR or the AAV9.RAM-d2tTA::TRE.EGFP virus mixed with the infection control virus
448 AAV9.CB.mCherry into dorsal hippocampus. Mice were anesthetized with 4% isoflurane and placed in a
449 stereotaxic apparatus, where they were kept under 1.5-2% isoflurane anesthesia (0.8-1 L/min), and
450 injected with buprenorphine (0.1 mg/kg) and carprofene (5 mg/kg) to prevent post-surgery pain. The
451 injection volume and flow rate (300 nl at 60 nl/min) were controlled with an injection micro-pump (World
452 Precision Instruments). Injection coordinates, using bregma as a reference point, were as follows: AP -
453 1.78, ML ± 2.40, DV -2.35. This site targets dorsal CA3b, but virus spreading resulted the infection of CA3a,
454 CA3b, CA3c, CA2 and in some cases few granule neurons and hilar cells of the DG. Mice were carefully
455 monitored for 4 days following surgery, and behavioral manipulation started after a recovery period of
456 approximately 2 weeks.

457 **Behavioral tests.** Once recovered, mice were single-housed to reduce uncontrolled experiences that could
458 contaminate the ensemble of CFC-related labelled engram cells. Then, mice were handled to habituate to

459 the experimenter for at least 3 consecutive days prior to CFC. Mice injected with the RAM virus were
460 deprived of doxycycline, switching to a regular diet, 48 hours before CFC training. On the one-trial learning
461 day, mice were transported in the experimental room and immediately placed in a novel conditioning
462 chamber enclosed in a sound-attenuating cabinet (Ugo Basile), enriched with visual cues, and allowed to
463 explore it for a total duration of 300s. After an initial exploration period, 3 mild foot-shocks (2s, 0.7 mA)
464 were delivered at a 150s, 210s, and 270s, leaving 30s for additional context sampling at the end. Mice
465 were recorded and freezing behavior was scored using ANY-Maze 6 software (Stoelting Europe). Freezing
466 was detected as the absence of movement apart from respiration, and freezing events were scored when
467 immobility lasted more than a threshold of 300ms. Mice were then returned to their home cage. For
468 context only (CO) exploration, mice were placed in a 50 cm x 50 cm custom-built open field, where some
469 objects were distributed. Mice were allowed to explore for 5 minutes before returned to their home cage.
470 The immediate shock test was carried out in the fear conditioning system. Mice explored the conditioning
471 chamber for only 2 seconds before receiving a 6-second-long foot-shock and were then returned to their
472 home cage.

473 **Histology.** Mice were anesthetized with intraperitoneal administration of a ketamine/xylazine mix (100
474 mg/kg/10 mg/kg) at different time intervals following CFC (1.5 h, 3 h, 4.5 h, 6 h, 12 h for c-Fos-ZsGreen1-
475 DR, 24 h for RAM). Mice were then intracardially perfused with 0.9% NaCl solution followed by 4%
476 paraformaldehyde (PFA) in 0.1 mM PBS. Brains were removed and postfixed in 4% PFA overnight at 4°C.
477 Brains were transferred in sucrose 30% in 0.1 mM PBS at 4°C until they sank. Brains were cut on a cryostat
478 into 25 µm-thick coronal sections and collected in PBS with 0.3% Triton X-100. Slices were immediately
479 mounted on glass slides and covered in DAPI-based mounting medium. The number of fluorescence
480 neurons was assessed directly without amplification.

481 **Confocal microscope**. Confocal acquisitions were performed using a Leica SP8 White Light Laser 2 on an
482 inverted stand (Leica Microsystems, Mannheim, Germany) and with a x20 (NA 0.75) immersion objective.
483 Images were analyzed using ImageJ. At least 5 slices per animal were acquired. Imaging of neuronal
484 cultures was carried out as well using confocal Leica SP8 White Light Laser 2 (Leica Microsystems,
485 Mannheim, Germany) and with a x20 (NA 0.75) immersion objective. In all experiments, the settings (laser
486 power, gain, offset) were fixed between groups as well as the pixel size (120 nm).

487 **Ex-vivo slice preparation.** Slices were prepared 3 hours or 24 hours following CFC for FLEN-injected mice
488 and RAM-injected mice respectively. To attempt to reduce stress-related unspecific c-Fos activation, mice
489 were anesthetized with a ketamine/xylazine mix (100 mg/kg/10 mg/kg; i.p.) and intracardially perfused

490 with an ice-cold oxygenated (95% O2 and 5% CO2) cutting solution containing (in mM): 87 NaCl, 2.5 KCl,
491 1.25 NaH2PO4, 25 NaHCO3, 25 glucose, 75 sucrose, 0.5 CaCl2, 7 MgCl2, pH 7.4, 315 mOsm/kg. Brains were
492 quickly dissected out and parasagittal slices from both hemispheres (300 µm thick) were cut on a
493 vibratome (Leica VT1200S, Germany) in the same oxygenated ice-cold cutting solution. Slices were then
494 incubated at 34°C in a resting chamber containing the same cutting solution for 20-30 minutes for
495 recovery. Slices were then transferred in a resting chamber filled with an oxygenated (95% O2 and 5%
496 CO2) artificial cerebrospinal fluid (aCSF) containing (mM): 125 NaCl, 2.5 KCl, 1.25 NaH2PO4, 26 NaHCO3,
497 1.3 MgCl2, 2.3 CaCl2, 10 glucose, pH 7.4, 300 mOsm/kg at room temperature for the rest of the day.

498 **Electrophysiology.** When transferred to a recording chamber, slices were continuously superfused with
499 aCSF. CA3 pyramidal cells were identified with an infrared differential interference contrast (IR-DIC)
500 microscope with a water immersion 63X objective (N.A. 0.8). Neurons were then classified as engram
501 neurons (simultaneous expression of ZsGreen1-DR/mCherry or EGFP/mCherry when RAM was used) or
502 non-engram neuron (mCherry expression only) with a 2p microscope. Whole-cell recordings were made
503 at room temperature using borosilicate glass capillaries with resistances between 4-6 MΩ. For current
504 clamp recordings, the intracellular solution contained (in mM): 135 K-gluconate, 5 KCl, 2 NaCl, 10 Na2-
505 phosphocreatine, 0.1 EGTA, 10 HEPES, 5 Mg-ATP, 0.4 Na-GTP, pH 7.2 adjusted with KOH, 280-290
506 mOsm/Kg. For voltage clamp mode, the patch pipettes were filled with a solution containing (mM): 140
507 Cs-methanesulfonate, 2 MgCl2, 4 NaCl, 5 Na-phosphocreatine, 0.2 EGTA, 10 HEPES, 3 Na2-ATP, 0.3 GTP,
508 pH 7.2 adjusted with CsOH, 280-290 mOsm/Kg. To record inhibitory currents, a high-chloride intracellular
509 solution was used, containing (mM): 103 CsCl, 12 $CsCH_3O_3S$, 5 TEA-Cl, 10 HEPES, 4 Mg-ATP, 0.5 Na-GTP, 1
510 $MgCl_2$, pH adjusted to 7.2 with CsOH, 280-290 mOsm/Kg. No liquid-junction correction was used. Neurons
511 were held at –70 mV. Leak current and series resistance were monitored throughout each experiment;
512 neurons with a leak current >200 pA and a series resistance >25MΩ or if these parameters changed more
513 than 20% were excluded from analysis. All recordings were performed 5-10 min after opening the
514 membrane. Input resistance was quantified by linearly fitting the voltage change against injected current.
515 Steps of hyper- and depolarizing current steps were injected to determine action potential threshold and
516 rheobase. Action potential firing pattern was determined by injecting 200 pA steps of current.
517 Spontaneous EPSCs (sEPSCs) were isolated by bath application of bicuculline (10 µM), while mEPSCs were
518 recorded in presence of bicuculline (10 µM) and tetrodotoxin (0.5 µM). Spontaneous IPSCs (sIPSCs) were
519 recorded in presence of D-AP5 (50 µM) and NBQX (20 µM), while mIPSCs were isolated in presence of D-
520 AP5 (50 µM), NBQX (20 µM) and TTX (0.5 µM). Spontaneous and miniature synaptic events were detected
521 using a deconvolution-based approach (Pernía-Andrade et al., 2012). To record evoked EPSCs (eEPSCs),

522 stimulating glass pipettes (World Precision Instruments) were filled with aCSF and placed in the hilus, close
523 to the granule cell layer to stimulate initial portion of Mf axons. Voltage pulses (200 µs) were delivered
524 through a stimulus isolator (Digitimer, UK). Stimulation intensity was adjusted to obtain minimal Mf
525 stimulation (Marchal and Mulle., 2004). Basal synaptic transmission was recorded while holding CA3
526 neurons at -70 mV with pulses delivered at a low frequency of 0.1 Hz. Frequency was then increased to 1
527 Hz to induce frequency facilitation. After 2-3 minutes, when facilitation was extinguished, the voltage was
528 switched to +5 mV (reversal potential for cations) to record di-synaptic eIPSC. All recordings were obtained
529 with a HEKA EPC10 amplifier, filtered at 3.3 kHz and digitized at 10 kHz via PatchMaster software
530 (Lambrecht, Germany). Data was analyzed offline using custom-made Python scripts.

531 **Statistical analysis and graphical representations.** Statistical analyses and graphical representation were
532 performed with custom-written Python codes. Data are presented as boxplots and scatter plots indicating
533 the number of samples per group. Boxplots indicate median, first and third quartiles and whiskers
534 represent the rest of the distribution. Bold horizontal and vertical lines on scattered data points represent
535 mean and SEM respectively. Values were first tested for normality (D'Agostino and Pearson omnibus test
536 or Shapiro-Wilk test). Normally distributed data were compared using a t-test (two-sided) while Mann–
537 Whitney rank test (two-sided) was used for non-normal data set. Multiple group comparison was carried
538 out using one-way ANOVA when data were normally distributed or Kruskalis-Wallis when normality did
539 not apply. Tukey's *post hoc* comparison analysis or Dunn *post hoc* comparison analysis was applied.
540 Cumulative frequency distributions and normalized distributions were tested using Kolmogorov-Smirnov
541 test. Statistical differences were considered as significant at $p < 0.05$.

542 **REFERENCES**

543 Bessières, B., Dupuis, J., Groc, L., Bontempi, B., & Nicole, O. (2024). Synaptic rearrangement of NMDA
544 receptors controls memory engram formation and malleability in the cortex. *Science Advances*, *10*(35).
545 https://doi.org/10.1126/sciadv.ado1148

546 DeNardo, L. A., Liu, C. D., Allen, W. E., Adams, E. L., Friedmann, D., Fu, L., Guenthner, C. J., Tessier-
547 Lavigne, M., & Luo, L. (2019). Temporal evolution of cortical ensembles promoting remote memory
548 retrieval. *Nature Neuroscience*, *22*(3), 460-469. https://doi.org/10.1038/s41593-018-0318-7

549 Denny, C. A., Kheirbek, M. A., Alba, E. L., Tanaka, K. F., Brachman, R. A., Laughman, K. B., Tomm, N. K.,
550 Turi, G. F., Losonczy, A., & Hen, R. (2014). Hippocampal Memory Traces Are Differentially Modulated by
551 Experience, Time, and Adult Neurogenesis. *Neuron*, *83*(1), 189-201.
552 https://doi.org/10.1016/j.neuron.2014.05.018

553 Ding, L., Chen, H., Diamantaki, M., Coletta, S., Preston-Ferrer, P., & Burgalossi, A. (2020). Structural
554 Correlates of CA2 and CA3 Pyramidal Cell Activity in Freely-Moving Mice. *The Journal of Neuroscience*,
555 *40*(30), 5797-5806. https://doi.org/10.1523/JNEUROSCI.0099-20.2020

556 Eichenbaum, H. (2000). A cortical–hippocampal system for declarative memory. *Nature Reviews*
557 *Neuroscience*, *1*(1), 41-50. https://doi.org/10.1038/35036213

558 Galimberti, I., Gogolla, N., Alberi, S., Santos, A. F., Muller, D., & Caroni, P. (2006). Long-Term
559 Rearrangements of Hippocampal Mossy Fiber Terminal Connectivity in the Adult Regulated by
560 Experience. *Neuron*, *50*(5), 749-763. https://doi.org/10.1016/j.neuron.2006.04.026

561 Goto, A., Bota, A., Miya, K., Wang, J., Tsukamoto, S., Jiang, X., Hirai, D., Murayama, M., Matsuda, T.,
562 McHugh, T. J., Nagai, T., & Hayashi, Y. (2021). Stepwise synaptic plasticity events drive the early phase of
563 memory consolidation. *Science*, *374*(6569), 857-863. https://doi.org/10.1126/science.abj9195

564 Han, J.-H., Kushner, S. A., Yiu, A. P., Hsiang, H.-L. (Liz), Buch, T., Waisman, A., Bontempi, B., Neve, R. L.,
565 Frankland, P. W., & Josselyn, S. A. (2009). Selective Erasure of a Fear Memory. *Science*, *323*(5920),
566 1492-1496. https://doi.org/10.1126/science.1164139

567 Henze, D. A., Wittner, L., & Buzsáki, G. (2002). Single granule cells reliably discharge targets in the
568 hippocampal CA3 network in vivo. *Nature Neuroscience*, *5*(8), 790-795. https://doi.org/10.1038/nn887

569 Holtmaat, A., & Caroni, P. (2016). Functional and structural underpinnings of neuronal assembly
570 formation in learning. *Nature Neuroscience*, *19*(12), 1553-1562. https://doi.org/10.1038/nn.4418

571 Humeau, Y., & Choquet, D. (2019). The next generation of approaches to investigate the link between
572 synaptic plasticity and learning. *Nature Neuroscience*, *22*(10), 1536-1543.
573 https://doi.org/10.1038/s41593-019-0480-6

574 Josselyn, S. A., & Tonegawa, S. (2020). Memory engrams : Recalling the past and imagining the future.
575 *Science*, *367*(6473), eaaw4325. https://doi.org/10.1126/science.aaw4325

576 Kamiya, H., & Ozawa, S. (1999). Dual mechanism for presynaptic modulation by axonal metabotropic
577 glutamate receptor at the mouse mossy fibre-CA3 synapse. *The Journal of Physiology*, *518*(2), 497-506.
578 https://doi.org/10.1111/j.1469-7793.1999.0497p.x

Kawashima, T., Kitamura, K., Suzuki, K., Nonaka, M., Kamijo, S., Takemoto-Kimura, S., Kano, M., Okuno, H., Ohki, K., & Bito, H. (2013). Functional labeling of neurons and their projections using the synthetic activity–dependent promoter E-SARE. *Nature Methods*, *10*(9), 889-895. https://doi.org/10.1038/nmeth.2559

Kesner, R. P., & Rolls, E. T. (2015). A computational theory of hippocampal function, and tests of the theory : New developments. *Neuroscience & Biobehavioral Reviews*, *48*, 92-147. https://doi.org/10.1016/j.neubiorev.2014.11.009

Kitamura, T., Ogawa, S. K., Roy, D. S., Okuyama, T., Morrissey, M. D., Smith, L. M., Redondo, R. L., & Tonegawa, S. (2017). Engrams and circuits crucial for systems consolidation of a memory. *Science*, *356*(6333), 73-78. https://doi.org/10.1126/science.aam6808

Li, X., Zhao, X., Fang, Y., Jiang, X., Duong, T., Fan, C., Huang, C.-C., & Kain, S. R. (1998). Generation of Destabilized Green Fluorescent Protein as a Transcription Reporter. *Journal of Biological Chemistry*, *273*(52), 34970-34975. https://doi.org/10.1074/jbc.273.52.34970

Liu, X., Ramirez, S., Pang, P. T., Puryear, C. B., Govindarajan, A., Deisseroth, K., & Tonegawa, S. (2012). Optogenetic stimulation of a hippocampal engram activates fear memory recall. *Nature*, *484*(7394), 381-385. https://doi.org/10.1038/nature11028

Lovett-Barron, M., Kaifosh, P., Kheirbek, M. A., Danielson, N., Zaremba, J. D., Reardon, T. R., Turi, G. F., Hen, R., Zemelman, B. V., & Losonczy, A. (2014). Dendritic Inhibition in the Hippocampus Supports Fear Learning. *Science*, *343*(6173), 857-863. https://doi.org/10.1126/science.1247485

Marchal, C., & Mulle, C. (2004). Postnatal maturation of mossy fibre excitatory transmission in mouse CA3 pyramidal cells : A potential role for kainate receptors. *The Journal of Physiology*, *561*(1), 27-37. https://doi.org/10.1113/jphysiol.2004.069922

Marneffe, C., Moreira-de-Sá, A., Lecomte, S., Erhardt, A., & Mulle, C. (2024). Short term plasticity at hippocampal mossy fiber synapses. *Neuroscience*, S0306452224004974. https://doi.org/10.1016/j.neuroscience.2024.09.044

Maruo, T., Mandai, K., Takai, Y., & Mori, M. (2016). Activity-dependent alteration of the morphology of a hippocampal giant synapse. *Molecular and Cellular Neuroscience*, *71*, 25-33. https://doi.org/10.1016/j.mcn.2015.12.005

Matz, M. V., Fradkov, A. F., Labas, Y. A., Savitsky, A. P., Zaraisky, A. G., Markelov, M. L., & Lukyanov, S. A. (1999). Fluorescent proteins from nonbioluminescent Anthozoa species. *Nature Biotechnology*, *17*(10), 969-973. https://doi.org/10.1038/13657

McNaughton, L. and Morris, R. G. M. (1987). Hippocampal synaptic enhancement and information storage within a distributed memory system. *Trends in Neuroscience, 10*(10).

Milczarek, M. M., Vann, S. D., & Sengpiel, F. (2018). Spatial Memory Engram in the Mouse Retrosplenial Cortex. *Current Biology*, *28*(12), 1975-1980.e6. https://doi.org/10.1016/j.cub.2018.05.002

Mocle, A. J., Ramsaran, A. I., Jacob, A. D., Rashid, A. J., Luchetti, A., Tran, L. M., Richards, B. A., Frankland, P. W., & Josselyn, S. A. (2024). Excitability mediates allocation of pre-configured ensembles to a hippocampal engram supporting contextual conditioned threat in mice. *Neuron*, *112*(9), 1487-1497.e6.

https://doi.org/10.1016/j.neuron.2024.02.007

Nakamura, N. H., Flasbeck, V., Maingret, N., Kitsukawa, T., & Sauvage, M. M. (2013). Proximodistal Segregation of Nonspatial Information in CA3 : Preferential Recruitment of a Proximal CA3-Distal CA1 Network in Nonspatial Recognition Memory. *Journal of Neuroscience*, *33*(28), 11506-11514. https://doi.org/10.1523/JNEUROSCI.4480-12.2013

Nakazawa, K., Quirk, M. C., Chitwood, R. A., Watanabe, M., Yeckel, M. F., Sun, L. D., Kato, A., Carr, C. A., Johnston, D., Wilson, M. A., & Tonegawa, S. (2002). Requirement for Hippocampal CA3 NMDA Receptors in Associative Memory Recall. *Science*, *297*(5579), 211-218. https://doi.org/10.1126/science.1071795

Nakazawa, K., Sun, L. D., Quirk, M. C., Rondi-Reig, L., Wilson, M. A., & Tonegawa, S. (2003). Hippocampal CA3 NMDA Receptors Are Crucial for Memory Acquisition of One-Time Experience. *Neuron*, *38*(2), 305-315. https://doi.org/10.1016/S0896-6273(03)00165-X

Nakazawa, Y., Pevzner, A., Tanaka, K. Z., & Wiltgen, B. J. (2016). Memory retrieval along the proximodistal axis of CA1 : PROXIMODISTAL CA1. *Hippocampus*, *26*(9), 1140-1148. https://doi.org/10.1002/hipo.22596

Pernía-Andrade, A. J., Goswami, S. P., Stickler, Y., Fröbe, U., Schlögl, A., & Jonas, P. (2012). A Deconvolution-Based Method with High Sensitivity and Temporal Resolution for Detection of Spontaneous Synaptic Currents In Vitro and In Vivo. *Biophysical Journal*, *103*(7), 1429-1439. https://doi.org/10.1016/j.bpj.2012.08.039

Pignatelli, M., Ryan, T. J., Roy, D. S., Lovett, C., Smith, L. M., Muralidhar, S., & Tonegawa, S. (2019). Engram Cell Excitability State Determines the Efficacy of Memory Retrieval. *Neuron*, *101*(2), 274-284.e5. https://doi.org/10.1016/j.neuron.2018.11.029

Raus Balind, S., Magó, Á., Ahmadi, M., Kis, N., Varga-Németh, Z., Lőrincz, A., & Makara, J. K. (2019). Diverse synaptic and dendritic mechanisms of complex spike burst generation in hippocampal CA3 pyramidal cells. *Nature Communications*, *10*(1), 1859. https://doi.org/10.1038/s41467-019-09767-w

Rebola, N., Carta, M., & Mulle, C. (2017). Operation and plasticity of hippocampal CA3 circuits : Implications for memory encoding. *Nature Reviews Neuroscience*, *18*(4), 208-220. https://doi.org/10.1038/nrn.2017.10

Reijmers, L. G., Perkins, B. L., Matsuo, N., & Mayford, M. (2007). Localization of a Stable Neural Correlate of Associative Memory. *Science*, *317*(5842), 1230-1233. https://doi.org/10.1126/science.1143839

Ruediger, S., Vittori, C., Bednarek, E., Genoud, C., Strata, P., Sacchetti, B., & Caroni, P. (2011). Learning-related feedforward inhibitory connectivity growth required for memory precision. *Nature*, *473*(7348), 514-518. https://doi.org/10.1038/nature09946

Ryan, T. J., Roy, D. S., Pignatelli, M., Arons, A., & Tonegawa, S. (2015). Engram cells retain memory under retrograde amnesia. *Science*, *348*(6238), 1007-1013. https://doi.org/10.1126/science.aaa5542

Sachidhanandam, S., Blanchet, C., Jeantet, Y., Cho, Y. H., & Mulle, C. (2009). Kainate Receptors Act as Conditional Amplifiers of Spike Transmission at Hippocampal Mossy Fiber Synapses. *The Journal of Neuroscience*, *29*(15), 5000-5008. https://doi.org/10.1523/JNEUROSCI.5807-08.2009

Sørensen, A. T., Cooper, Y. A., Baratta, M. V., Weng, F.-J., Zhang, Y., Ramamoorthi, K., Fropf, R., LaVerriere, E., Xue, J., Young, A., Schneider, C., Gøtzsche, C. R., Hemberg, M., Yin, J. C., Maier, S. F., & Lin, Y. (2016). A robust activity marking system for exploring active neuronal ensembles. *eLife*, *5*, e13918. https://doi.org/10.7554/eLife.13918

Sun, Q., Sotayo, A., Cazzulino, A. S., Snyder, A. M., Denny, C. A., & Siegelbaum, S. A. (2017). Proximodistal Heterogeneity of Hippocampal CA3 Pyramidal Neuron Intrinsic Properties, Connectivity, and Reactivation during Memory Recall. *Neuron*, *95*(3), 656-672.e3. https://doi.org/10.1016/j.neuron.2017.07.012

Sun, X., Bernstein, M. J., Meng, M., Rao, S., Sørensen, A. T., Yao, L., Zhang, X., Anikeeva, P. O., & Lin, Y. (2020). Functionally Distinct Neuronal Ensembles within the Memory Engram. *Cell*, *181*(2), 410-423.e17. https://doi.org/10.1016/j.cell.2020.02.055

Takeuchi, T., Duszkiewicz, A. J., & Morris, R. G. M. (2014). The synaptic plasticity and memory hypothesis : Encoding, storage and persistence. *Philosophical Transactions of the Royal Society B: Biological Sciences*, *369*(1633), 20130288. https://doi.org/10.1098/rstb.2013.0288

Thompson, L. T., Moyer, J. R., & Disterhoft, J. F. (1996). Transient changes in excitability of rabbit CA3 neurons with a time course appropriate to support memory consolidation. *Journal of Neurophysiology*, *76*(3), 1836-1849. https://doi.org/10.1152/jn.1996.76.3.1836

Tomé, D. F., Zhang, Y., Aida, T., Mosto, O., Lu, Y., Chen, M., Sadeh, S., Roy, D. S., & Clopath, C. (2024). Dynamic and selective engrams emerge with memory consolidation. *Nature Neuroscience*, *27*(3), 561-572. https://doi.org/10.1038/s41593-023-01551-w

Tonegawa, S., Liu, X., Ramirez, S., & Redondo, R. (2015). Memory Engram Cells Have Come of Age. *Neuron*, *87*(5), 918-931. https://doi.org/10.1016/j.neuron.2015.08.002

Torborg, C. L., Nakashiba, T., Tonegawa, S., & McBain, C. J. (2010). Control of CA3 Output by Feedforward Inhibition Despite Developmental Changes in the Excitation–Inhibition Balance. *The Journal of Neuroscience*, *30*(46), 15628-15637. https://doi.org/10.1523/JNEUROSCI.3099-10.2010

Tulving, E. (2002). Episodic Memory : From Mind to Brain. *Annual Review of Psychology*, *53*(1), 1-25. https://doi.org/10.1146/annurev.psych.53.100901.135114

Vandael, D., & Jonas, P. (2024). Structure, biophysics, and circuit function of a “giant” cortical presynaptic terminal. *Science*, *383*(6687), eadg6757. https://doi.org/10.1126/science.adg6757

Vetere, G., Tran, L. M., Moberg, S., Steadman, P. E., Restivo, L., Morrison, F. G., Ressler, K. J., Josselyn, S. A., & Frankland, P. W. (2019). Memory formation in the absence of experience. *Nature Neuroscience*, *22*(6), 933-940. https://doi.org/10.1038/s41593-019-0389-0

Weng, F.-J., Garcia, R. I., Lutzu, S., Alviña, K., Zhang, Y., Dushko, M., Ku, T., Zemoura, K., Rich, D., Garcia-Dominguez, D., Hung, M., Yelhekar, T. D., Sørensen, A. T., Xu, W., Chung, K., Castillo, P. E., & Lin, Y. (2018). Npas4 Is a Critical Regulator of Learning-Induced Plasticity at Mossy Fiber-CA3 Synapses during Contextual Memory Formation. *Neuron*, *97*(5), 1137-1152.e5. https://doi.org/10.1016/j.neuron.2018.01.026

Yap, E.-L., Pettit, N. L., Davis, C. P., Nagy, M. A., Harmin, D. A., Golden, E., Dagliyan, O., Lin, C., Rudolph,

692 S., Sharma, N., Griffith, E. C., Harvey, C. D., & Greenberg, M. E. (2021). Bidirectional perisomatic
693 inhibitory plasticity of a Fos neuronal network. *Nature*, *590*(7844), 115-121.
694 https://doi.org/10.1038/s41586-020-3031-0

695 Yiu, A. P., Mercaldo, V., Yan, C., Richards, B., Rashid, A. J., Hsiang, H.-L. L., Pressey, J., Mahadevan, V.,
696 Tran, M. M., Kushner, S. A., Woodin, M. A., Frankland, P. W., & Josselyn, S. A. (2014). Neurons Are
697 Recruited to a Memory Trace Based on Relative Neuronal Excitability Immediately before Training.
698 *Neuron*, *83*(3), 722-735. https://doi.org/10.1016/j.neuron.2014.07.017

699 Zhang, W., & Linden, D. J. (2003). The other side of the engram : Experience-driven changes in neuronal
700 intrinsic excitability. *Nature Reviews Neuroscience*, *4*(11), 885-900. https://doi.org/10.1038/nrn1248

701 Zucca, S., Griguoli, M., Malézieux, M., Grosjean, N., Carta, M., & Mulle, C. (2017). Control of Spike
702 Transfer at Hippocampal Mossy Fiber Synapses *In Vivo* by $GABA_A$ and $GABA_B$ Receptor-Mediated
703 Inhibition. *The Journal of Neuroscience*, *37*(3), 587-598. https://doi.org/10.1523/JNEUROSCI.2057-
704 16.2016

705 **Legends – Main Figures**

706 **Figure 1. Development of a novel viral tool to study early changes in the properties of CA3 engram cells**.
707 (**A**) Scheme representing the maturation of engram neurons during memory formation. Top panel: during
708 learning, a neuron receives numerous synaptic inputs, resulting in sequences of action potentials. This
709 activity triggers the rapid expression of immediate early genes (IEGs), marking the neuron as part of an
710 engram (yellow). As the engram matures (green), IEGs expression is not detectable anymore, yet the
711 neuron retains established engram properties. Bottom panel: expression function of IEG-based construct
712 to investigate and compare early and late engram properties. A construct with rapid offset (yellow) best
713 captures engrams shortly after learning, whereas a progressively expressing construct best captures more
714 mature engrams. (**B**) FLEN construct (c-Fos.ZsGreen1-DR) encapsulated in AAV2/9 vector. Bottom panel:
715 representative images showing ZsGreen1 fluorescence in c-Fos+ neurons (arrowhead) and c-Fos- neurons
716 (arrow). Scalebar = 50 µm. (**C**) Timeline of *in vitro* experiments to determine FLEN expression and offset
717 time course. After infection (DIV3) and activation (DIV11), samples are washed with a blocking medium
718 and images are acquired at different intervals (downward arrows). (**D**) Percentage of ZsGreen+ vs. all
719 transduced neurons (mCherry+ cells) at the different intervals following activation. (**E**) Representative
720 images of activated cultured neurons at 1, 2, 3, 4.5 and 6 hours after activation. Scalebar = 100 µm.

721 **Figure 2. *In vivo* FLEN labeling and decay time course following a salient experience.** (**A**) FLEN and an
722 infection marker viral vectors are injected bilaterally into CA3. Mice undergo contextual fear conditioning
723 (CFC), and sections are collected (downward arrows) 1.5, 3, 4.5, 6 and 12 hours following CFC. As a control,
724 sections are obtained from mice left undisturbed in their home cage (HC). (**B**) Left: one-time CFC
725 experiment scheme. Mice explore an arena for 5 minutes, 3 foot-shocks are given at 180, 210 and 270
726 seconds after the start of the test (red line). Top-right: paired comparison of the percentage of time mice
727 spent freezing during training and when replaced in the conditioning arena 1 hour after CFC. Bottom-right:
728 comparison of the percentage of time mice spent freezing during training, when placed in a different
729 neutral environment and 24 hours after CFC. These experiments show that the CA3-dependent shock-
730 context association is rapidly learned (within 1 hour), is highly environment-selective and it is retained for
731 24 hours. (**C**) Representative images of CA3 neurons expressing the infection marker (mCherry+, indicated
732 by arrow) and neurons expressing both the infection marker and FLEN (ZsGreen1+/mCherry+, indicated
733 by arrowhead). The latter are considered FLEN+ neurons. Scalebar = 50 µm. (**D**) Percentage of ZsGreen+
734 CA3 neurons over the total number of mCherry+ neurons at different intervals following activation. (**E**)
735 Representative sections of CFC-trained mice compared to HC untrained mice at different intervals

following CFC. Dashed lines outline the dentate gyrus (DG) cellular layer, while the dashed segment indicates the separation between CA3 and CA2. Scale bar = 100 µm. (**F**) Left panel: Schematic representation of neuronal position along the proximodistal axis analysis of CA3. The CA3 pyramidal layer was straightened and the x position of FLEN+ cells was normalized on a 0 (closer to DG) to 1 (closer to CA2) scale. Right panel: comparison of normalized proximodistal frequency distribution of CA3 FLEN+ cells placement in HC mice (gray) and 3 hours post-CFC mice (yellow). Bold lines represent the median of the respective distributions. HC median is displayed in the CFC plot to highlight distribution difference.

Figure 3. Electrophysiological analysis of intrinsic properties of CA3 engram neurons. (**A**) Experimental outline: mice were injected with either FLEN or RAM construct, subjected to CFC and then sacrificed at either 3- or 24-hours post-conditioning to collect acute hippocampal slices. Right: representative images of FLEN+ and RAM+ cells targeted for patch clamp recordings, with neighboring control FLEN- or RAM- neurons. Scale bar = 20 µm. (**B**) Membrane potential response. Left panel: representative membrane potential trace in response to incremental injected current in control cells (gray) and engram cells (yellow for FLEN and green for RAM). Right panel: graphs of input resistance for comparison between engram cells and their corresponding control cells. (**C**) Action potential firing pattern. Left panel: sample traces of long (1 second) above-rheobase current step to analyze the pattern of action potential firing current in control cells (gray) and engram cells (yellow and green). Right panel: average spike frequency graphs. (**D**) Cumulative spike frequency curve over the 1 second current step shown in (C) showing a similar distribution between FLEN+ and FLEN – neurons (top), and a more sustained firing of RAM+ compared to their RAM- neurons (bottom). (**E**) Left panel: difference between isolated spikes and bursts. A group of action potential is considered a burst if two or more spikes occur within a 50 ms interval. Right panel: stacked bar plot showing the fraction of bursting cells in each group.

Figure 4. Analysis of spontaneous EPSCs in CA3 engram neurons (**A**) Sample traces and cumulative distributions of sEPSCs recorded from CA3 engram neurons (FLEN in yellow, RAM in green). Top-left: comparison of spontaneous EPSCs (sEPSCs) between FLEN+ and FLEN- neurons, showing no difference in average amplitude, and representative traces showing differences in the frequency of sEPSCs between FLEN- and FLEN+ neurons. Top-center and top-right: cumulative frequency distribution of amplitude and inter-event interval (IEI) as a readout of sEPSC frequency in FLEN+ and FLEN- neurons. Bottom-left: comparison of spontaneous EPSCs between RAM+ and RAM- neurons showing no difference in average amplitude and sample traces showing differences in the frequency of sEPSCs between RAM+ and RAM- neurons. Bottom-center and bottom-right: cumulative frequency distribution of amplitude and inter-

767 event interval (IEI) of RAM+ and RAM- neurons. (**B**) The same as in (A) but for miniature EPSCs. Inset within
768 cumulative distribution of amplitude plot represent the normalized fraction of mEPSC larger than 40 pA,
769 likely due to giant mossy fiber activity.

770 **Figure 5. Analysis of spontaneous IPSCs in CA3 engram neurons** (**A**) Sample traces and cumulative
771 distributions of mIPSCs recorded from hippocampal CA3 engram (FLEN in yellow, RAM in green). Top-left:
772 comparison of the average miniature IPSC between FLEN+ and FLEN- neurons showing no difference in
773 amplitude. Below, sample traces of FLEN+ and FLEN- neurons showing differences in the frequency of
774 mIPSCs. Top-center and top-right: cumulative distribution plots for amplitude and inter-event interval (IEI)
775 in FLEN+ versus FLEN- neurons. Bottom-left: sample traces highlighting the difference in mIPSC frequency
776 between RAM- and RAM+ neurons. Below, sample traces of FLEN+ and FLEN- neurons showing difference
777 in the frequency of mIPSCs. Bottom-center and bottom-right: cumulative frequency distribution for
778 amplitude and inter-event interval (IEI) of RAM+ and RAM- neurons.

779 **Figure 6. Properties of Mf-CA3 synapses in CA3 engram neurons** (**A**) Schematic representation of Mf-CA3
780 EPSCs and feedfoward inhibition recordings. (**B**) Left panel: representative traces showing EPSC amplitude
781 in FLEN- (gray) and FLEN+ (yellow) cells following low frequency stimulation (0.1 Hz) and corresponding
782 increase evoked with a higher stimulation frequency (1 Hz), due to a presynaptic form of synaptic plasticity
783 characteristics of Mf-CA3 synapses (frequency facilitation). Center panel: amplitude plot for FLEN- and
784 FLEN+ stimulated at 0.1 Hz and 1 Hz. Right panel: frequency facilitation ratio plot shows no difference
785 between FLEN- and FLEN+ neurons. (**C**) Left panel: representative traces showing Mf-driven IPSCs
786 (feedforward inhibition) and EPSCs (direct excitatory activity) recorded in individual FLEN- (gray) and
787 FLEN+ (yellow) neurons. Center panel: amplitude plot of EPSCs and IPSCs for FLEN- and FLEN+ neurons.
788 Right panel: graph showing excitation-to-inhibition ratio, comparing FLEN- and FLEN+ neurons.

789 **Legends Supplementary Figures**

790 **Figure S1.** (**A**) Left panel: context-only and immediate-shock behavioral test layout. In the context-only
791 (CO) task, mice freely explore an arena without being conditioned; mice subjected to the immediate-shock
792 (IS) experience a long (8 seconds) foot-shock immediately after being placed in the conditioning cage,
793 preventing them exploring the environment and forming contextual memories. Right panel: plot
794 comparing the percentage of FLEN+ cells in the home cage group (from Figure 2D) and the context-only
795 and immediate-shock groups.

796 **Figure S2.** (**A**) Normalized proximodistal (x) and superficial-to-deep (y) frequency distribution of the
797 position of CA3 FLEN+ neurons in all behavioral groups. Black dashed lines indicate each group's median
798 value, while red dashed line represents the home cage group's median value. Each plot includes the
799 scattered x-y position of FLEN+ cells within the pyramidal layer, and the frequency distribution along the
800 proximodistal (top) and superficial-to-deep (right) axis.

801 **Figure S3.** (**A**) RAM construct outline and expression mechanism. Top panel: Dox administration prevents
802 binding of tTA protein to the TRE promoter, whereas Dox deprivation allows downstream EGFP
803 transcription. Bottom panel: scheme for *in vivo* experiments using the RAM system. Dox-fed mice are
804 bilaterally injected in CA3 with viral constructs for RAM and the infection marker AAV-CB7-mCherry. The
805 diet is switched to regular food chow 48 hours prior to the CFC. Then, mice undergo CFC and sections are
806 collected (downward arrows) 24 hours later and compared to untrained mice that never left their home
807 cage. (**B**) Percentage of RAM+ CA3 neurons over the total number of mCherry+ neurons in HC and 24
808 hours post-CFC. (**C**) Representative sections of CFC-trained mice compared to HC mice. Dashed lines
809 outline the dentate gyrus (DG) cellular layer, while the dashed segment indicates the separation between
810 CA3 and CA2. Scale bar = 100 µm.

811 **Figure S4.** (**A**) Left panel: overview of action potential features analyzed. Right panel: Initial frequency
812 calculation. (**B** and **C**) Summary of analyzed action potential properties in FLEN+ vs. FLEN- (B) and RAM+
813 vs. RAM- (C).

814 **Table 1.**

	FLEN			RAM		
	FLEN-	**FLEN+**	**Test**	**RAM-**	**RAM+**	**Test**
Peak (mV)	45.19 ± 2.25, n=19	43.92 ± 4.62, n=9	Mann-Whitney U, p=1.00	47.93 ± 1.41, n=15	50.91 ± 1.57, n=13	T-test, p=0.17
Threshold (mV)	-40.41 ± 1.54, n=20	-42.47 ± 1.36, n=14	T-test, p=0.35	-41.53 ± 1.35, n=15	-39.78 ± 2.46, n=13	T-test, p=0.52
Amplitude (mV)	99.91 ± 4.63, n=19	98.67 ± 8.73, n=9	T-test, p=0.89	103.71 ± 3.93, n=15	101.18 ± 4.53, n=13	T-test, p=0.67
Width (ms)	0.002 ± 0.001, n=16	0.002 ± 0.001, n=6	Mann-Whitney U, p=0.51	0.0017 ± 0.0001, n=13	0.0016 ± 0.00003, n=7	Mann-Whitney U, p=0.36
Upstroke (mV/s)	197.06 ± 19.54, n=19	213.35 ± 35.48, n=9	T-test, p=0.67	229.89 ± 17.86, n=15	241.65 ± 23.2, n=13	T-test, p=0.69
Downstroke (mV/s)	-57.99 ± 7.91, n=19	-54.99 ± 6.18, n=9	Mann-Whitney U, p=0.84	-56.70 ± 4.43, n=15	-59.96 ± 3.62, n=13	T-test, p=0.58
Initial frequency (Hz)	21.58 ± 4.15, n=16	25.04 ± 12.83, n=7	Mann-Whitney U, p=0.62	41.74 ± 9.54, n=10	25.30 ± 6.43, n=11	Mann-Whitney U, p=0.25
ISI (ms)	0.19 ± 0.05, n=16	0.26 ± 0.08, n=7	Mann-Whitney U, p=0.28	0.14 ± 0.02, n=10	0.14 ± 0.02, n=11	T-test, p=0.98

815

Figure 1

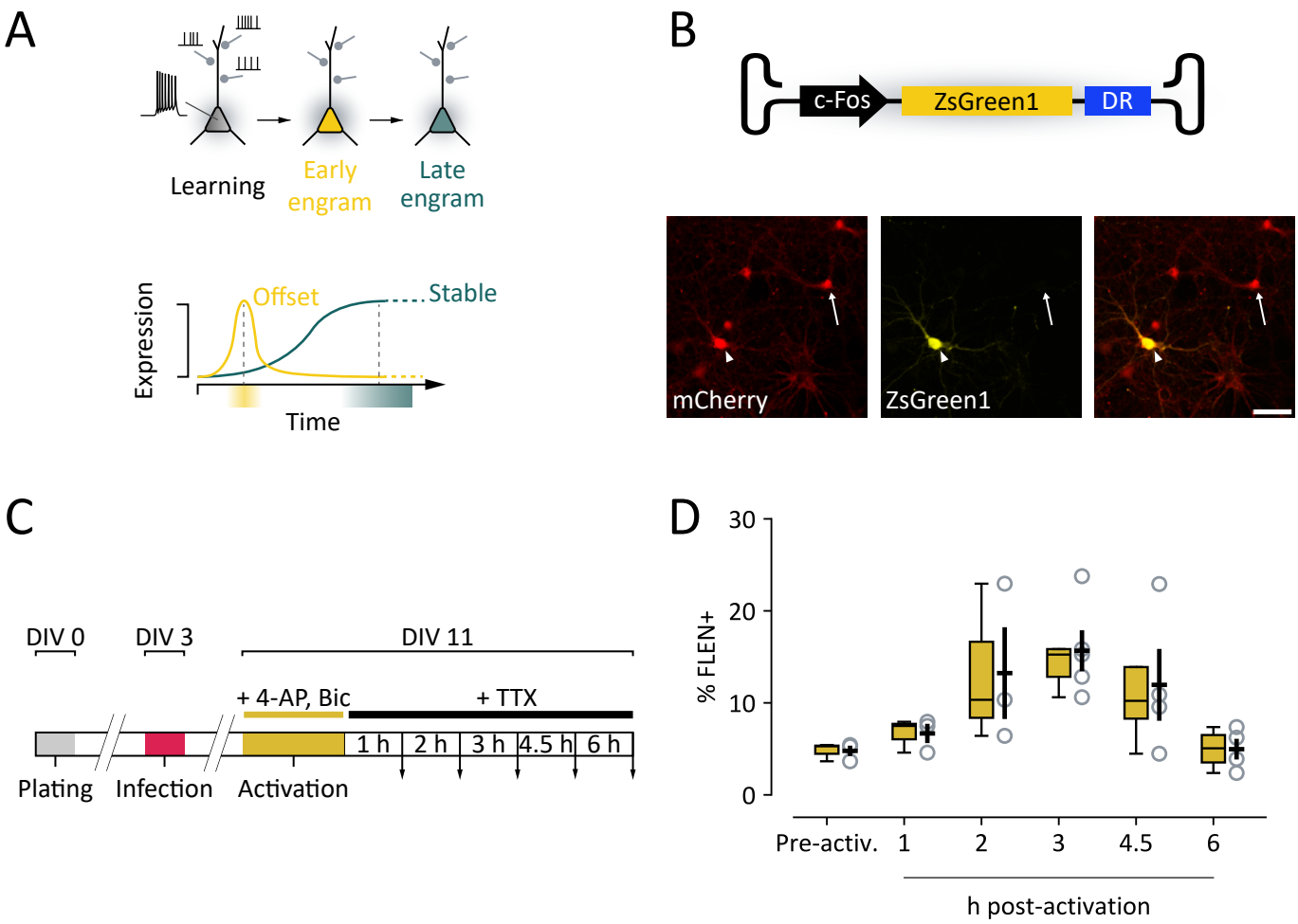
A
Learning
Early engram
Late engram
Expression
Offset
Stable
Time
B
c-Fos
ZsGreen1
DR
mCherry
ZsGreen1
C
DIV 0
DIV 3
DIV 11
+ 4-AP, Bic
+ TTX
1 h
2 h
3 h
4.5 h
6 h
Plating
Infection
Activation
D
% FLEN+
30
20
10
0
Pre-activ.
1
2
3
4.5
6
h post-activation

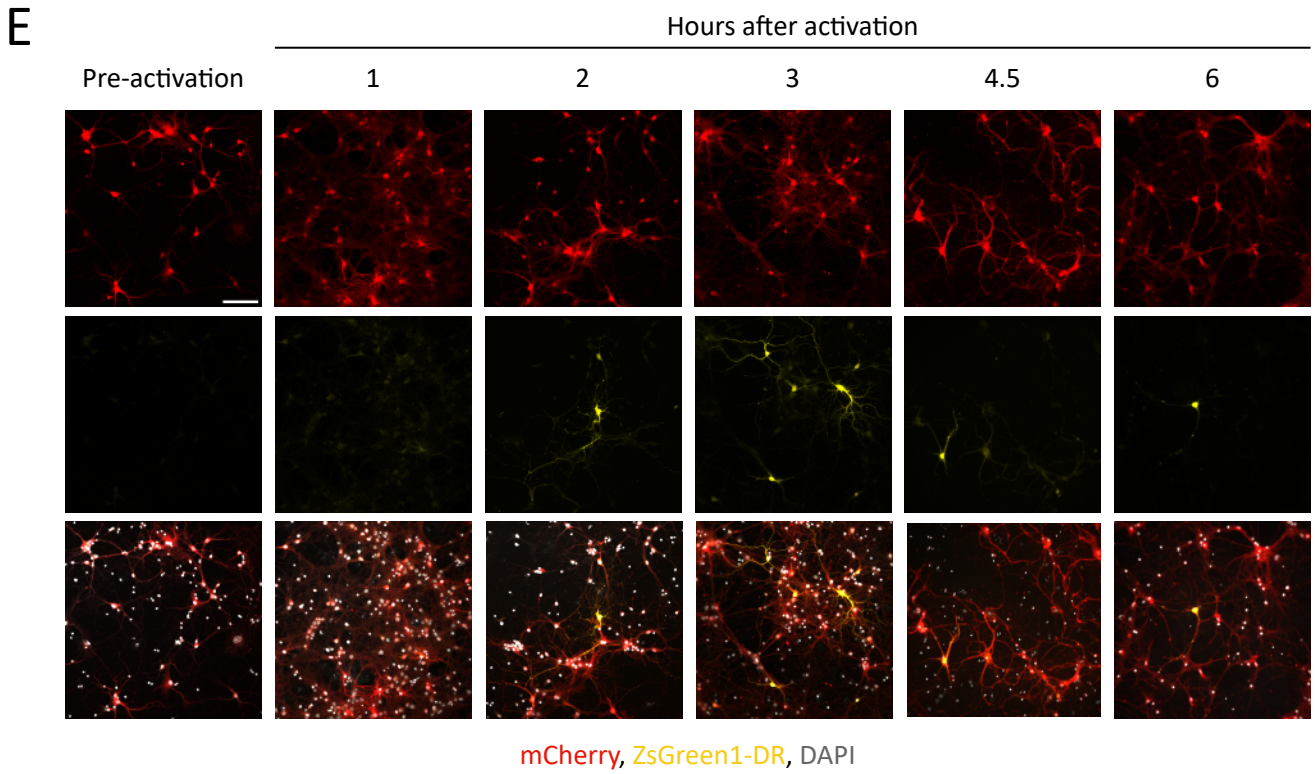
E
Hours after activation
Pre-activation
1
2
3
4.5
6
mCherry, ZsGreen1-DR, DAPI

Figure 2

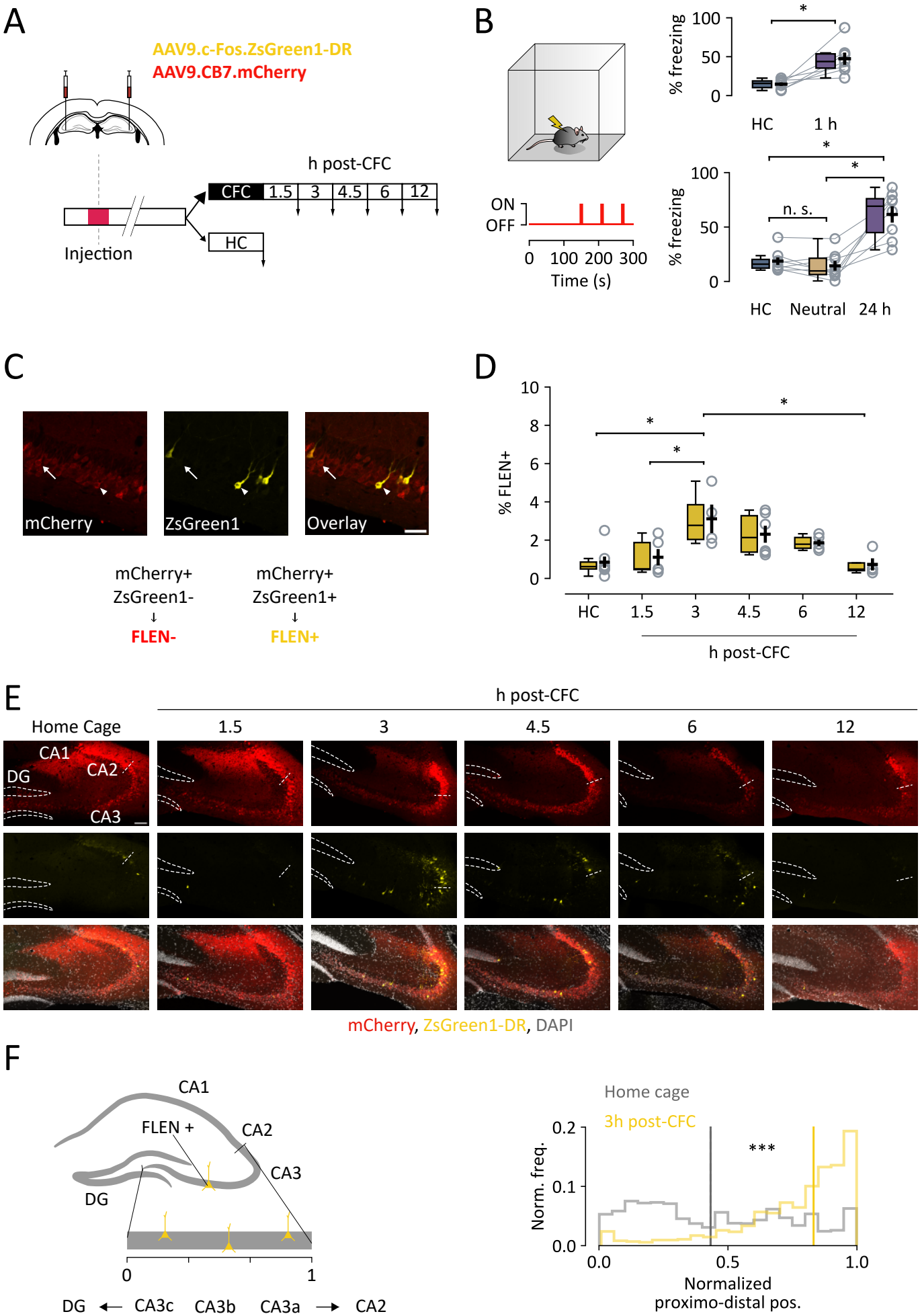
A
AAV9.c-Fos.ZsGreen1-DR
AAV9.CB7.mCherry
h post-CFC
CFC
1.5
3
4.5
6
12
HC
Injection
B
ON
OFF
0
100
200
300
Time (s)
% freezing
100
50
0
*
HC
1 h
*
*
n. s.
HC
Neutral
24 h
C
mCherry
ZsGreen1
Overlay
mCherry+
ZsGreen1-
FLEN-
mCherry+
ZsGreen1+
FLEN+
D
% FLEN+
10
8
6
4
2
0
HC
1.5
3
4.5
6
12
h post-CFC
E
h post-CFC
Home Cage
1.5
3
4.5
6
12
CA1
CA2
DG
CA3
mCherry, ZsGreen1-DR, DAPI
F
CA1
FLEN +
CA2
CA3
DG
0
1
DG ← CA3c CA3b CA3a → CA2
Home cage
3h post-CFC
Norm. freq.
0.2
0.1
0.0
***
0.0
0.5
1.0
Normalized
proximo-distal pos.

Figure 3

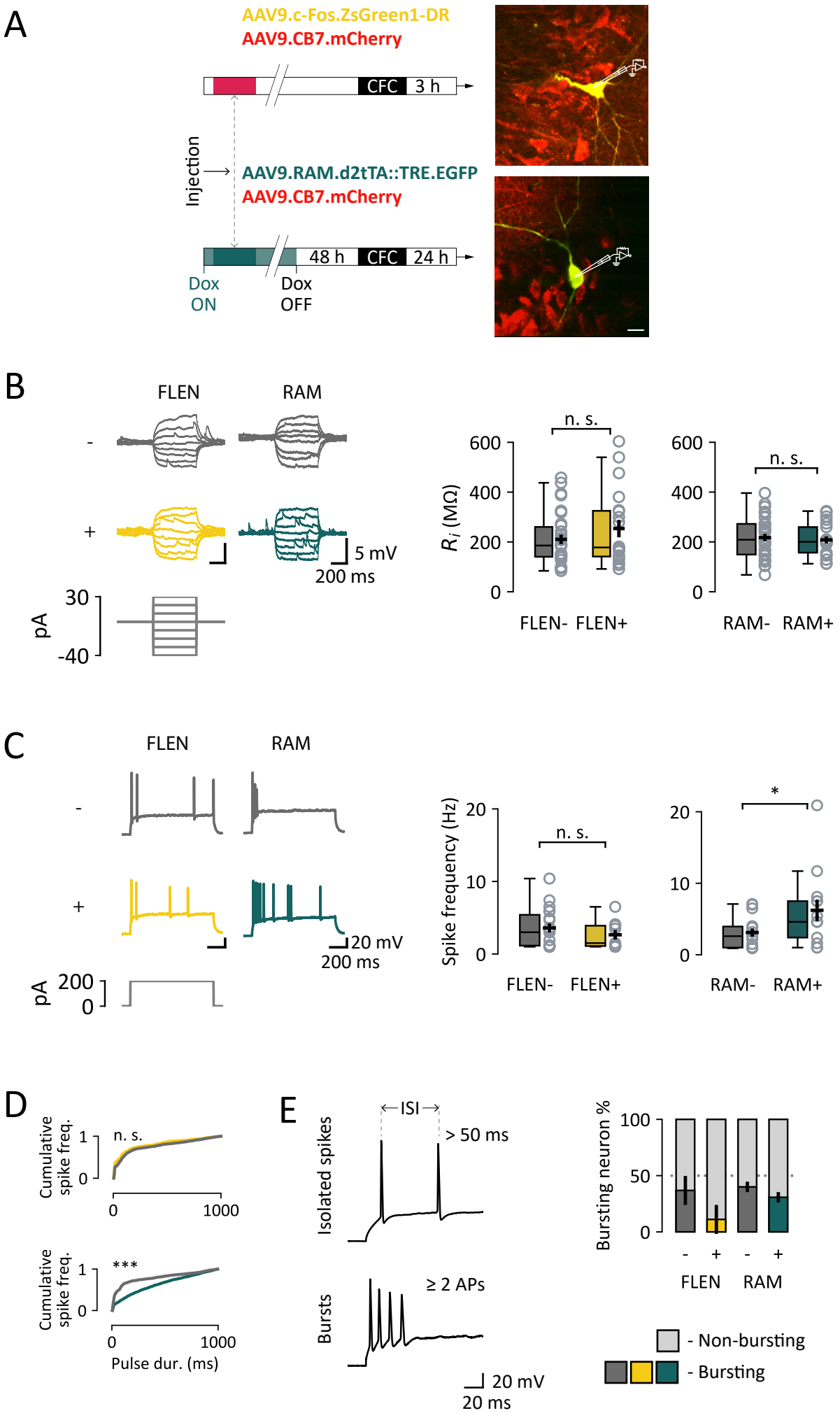
A
AAV9.c-Fos.ZsGreen1-DR
AAV9.CB7.mCherry
CFC
3 h
Injection
AAV9.RAM.d2tTA::TRE.EGFP
AAV9.CB7.mCherry
48 h
CFC
24 h
Dox ON
Dox OFF
B
FLEN
RAM
-
+
5 mV
200 ms
pA
30
-40
n. s.
R_i (MΩ)
600
400
200
0
FLEN-
FLEN+
RAM-
RAM+
C
FLEN
RAM
20 mV
200 ms
200
0
Spike frequency (Hz)
20
10
*
D
Cumulative spike freq.
1
0
n. s.
1000
***
Pulse dur. (ms)
E
Isolated spikes
ISI
> 50 ms
Bursts
≥ 2 APs
20 mV
20 ms
Bursting neuron %
100
50
FLEN
RAM
- Non-bursting
- Bursting

Figure 4

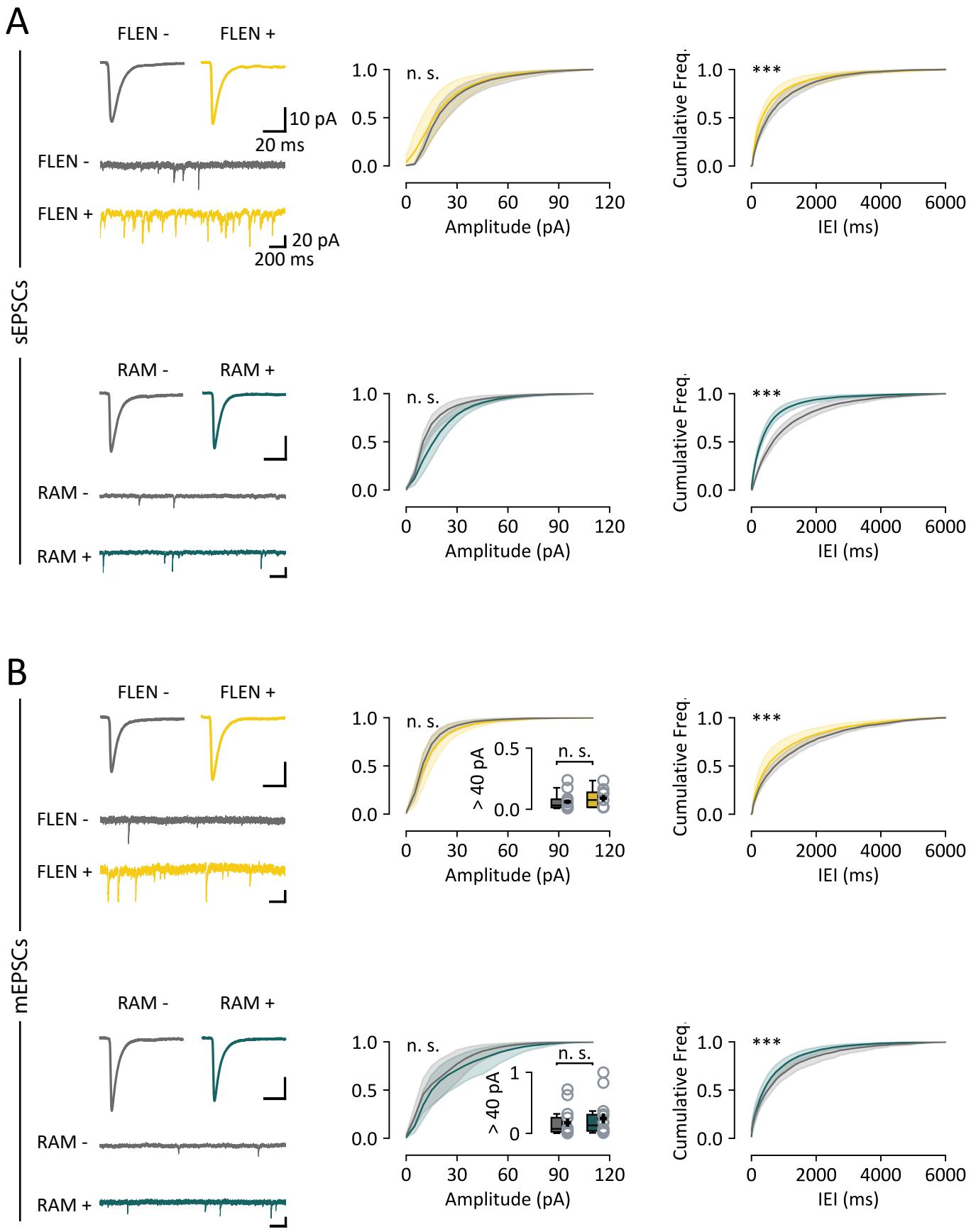
A
FLEN -
FLEN +
10 pA
20 ms
FLEN -
FLEN +
20 pA
200 ms
sEPSCs
RAM -
RAM +
RAM -
RAM +
n. s.
1.0
0.5
0.0
0
30
60
90
120
Amplitude (pA)
Cumulative Freq.
***
0
2000
4000
6000
IEI (ms)
B
mEPSCs
> 40 pA
0.5
0.0
1
0

Figure 5

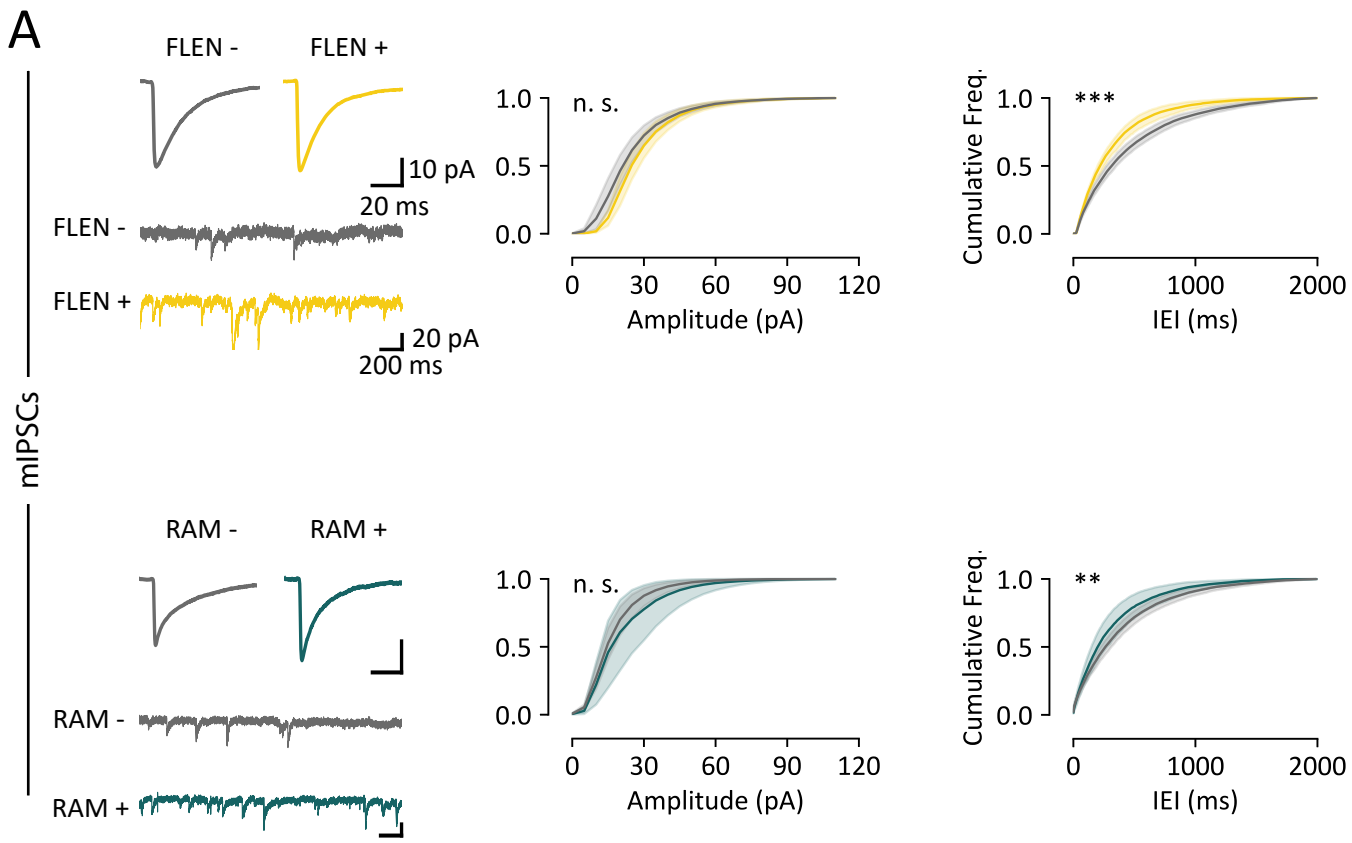
A
mIPSCs
FLEN -
FLEN +
10 pA
20 ms
FLEN -
FLEN +
20 pA
200 ms
n. s.
1.0
0.5
0.0
0
30
60
90
120
Amplitude (pA)
Cumulative Freq.
***
1000
2000
IEI (ms)
RAM -
RAM +
RAM -
RAM +
n. s.
**

Figure 6

A

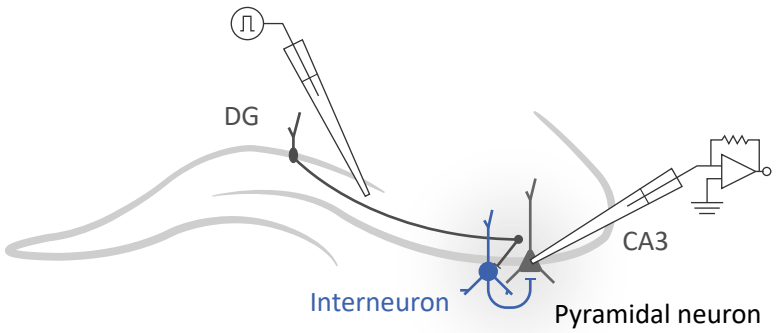
DG
CA3
Interneuron
Pyramidal neuron

B

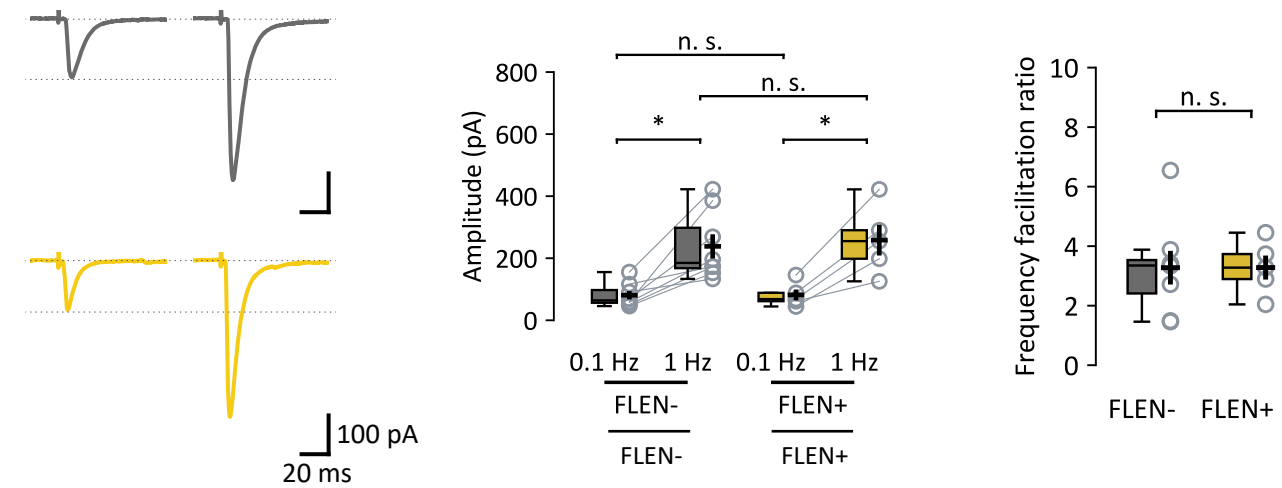
100 pA
20 ms
Amplitude (pA)
800
600
400
200
0
n. s.
n. s.
*
*
0.1 Hz
1 Hz
0.1 Hz
1 Hz
FLEN-
FLEN-
FLEN+
FLEN+
Frequency facilitation ratio
10
8
6
4
2
0
n. s.
FLEN-
FLEN+

C

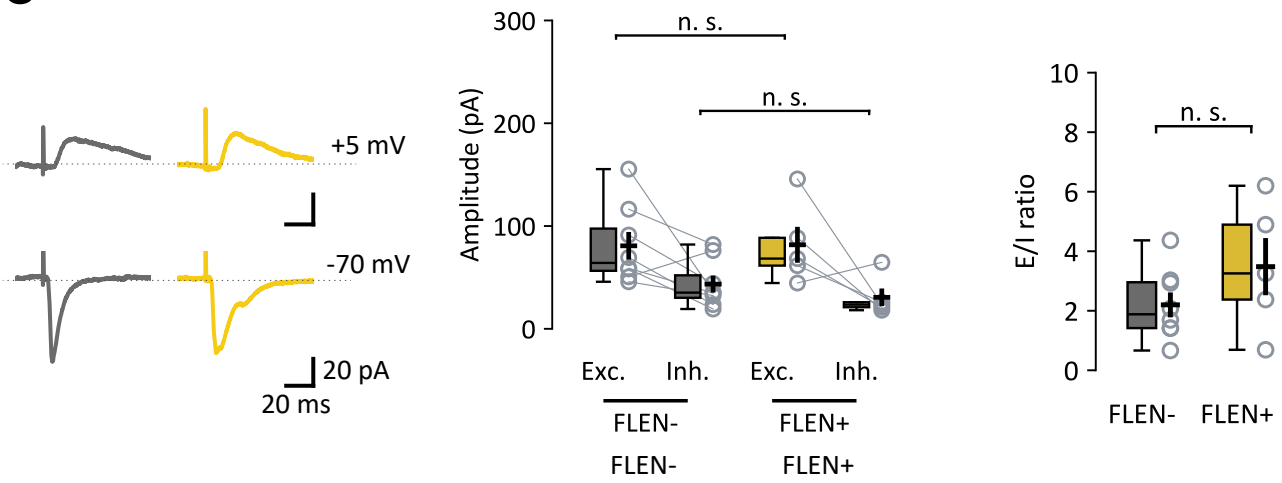
+5 mV
-70 mV
20 pA
20 ms
Amplitude (pA)
300
200
100
0
n. s.
n. s.
Exc.
Inh.
Exc.
Inh.
FLEN-
FLEN-
FLEN+
FLEN+
E/I ratio
10
8
6
4
2
0
n. s.
FLEN-
FLEN+

Figure S1

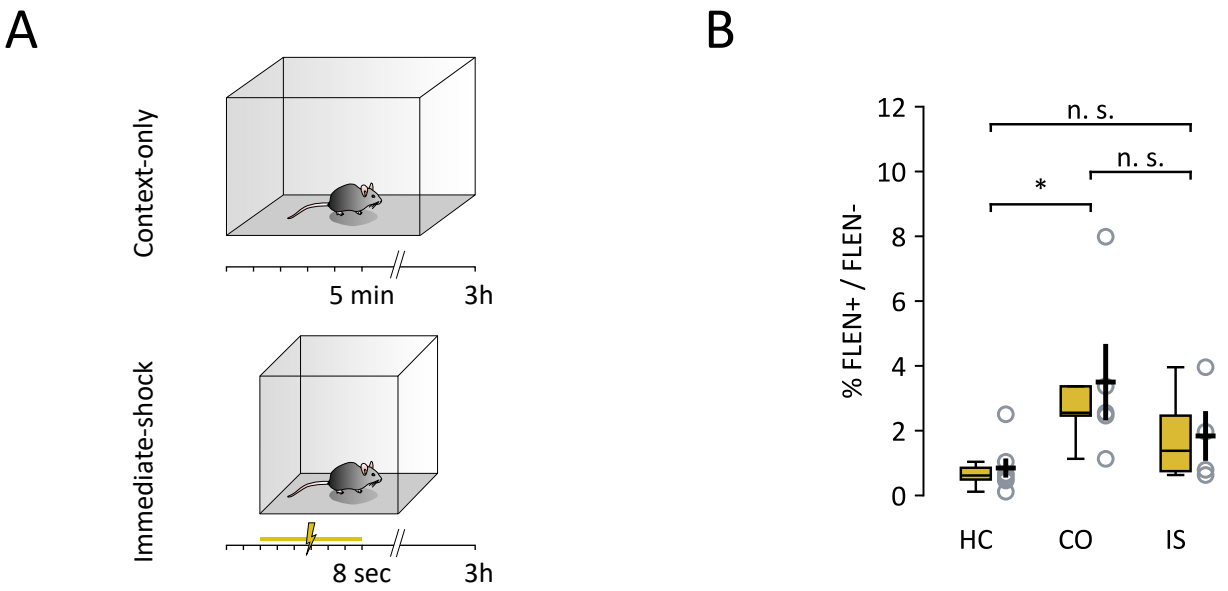
A
Context-only
5 min
3h
Immediate-shock
8 sec
3h
B
% FLEN+ / FLEN-
12
10
8
6
4
2
0
n. s.
n. s.
*
HC
CO
IS

Figure S2

A

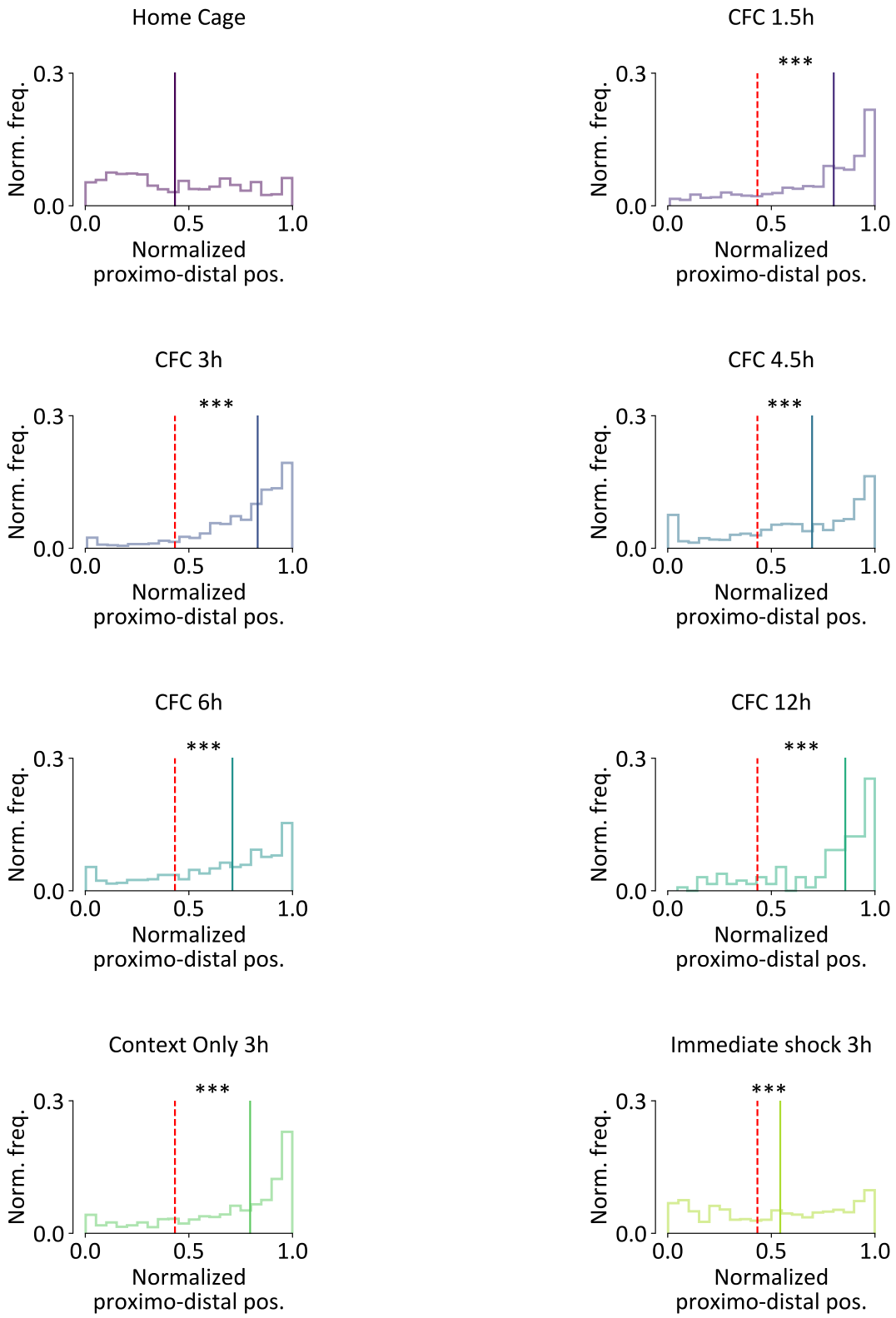
Home Cage
CFC 1.5h
CFC 3h
CFC 4.5h
CFC 6h
CFC 12h
Context Only 3h
Immediate shock 3h
Norm. freq.
0.3
0.0
0.0
0.5
1.0
Normalized
proximo-distal pos.
***

Figure S3

A

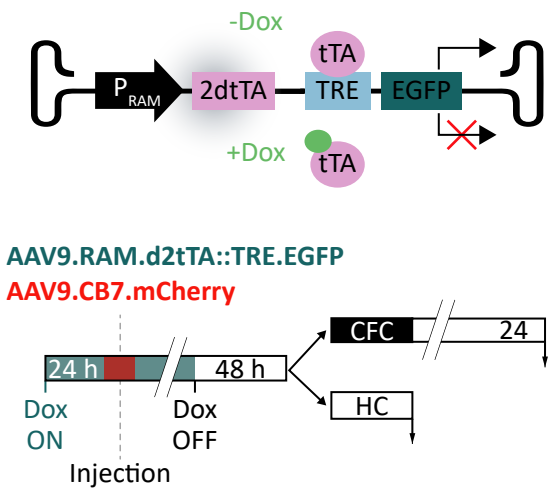

B

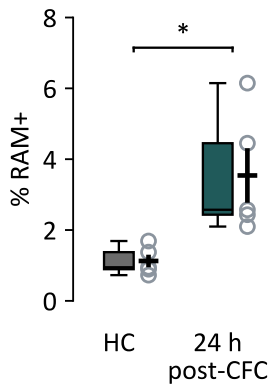

C

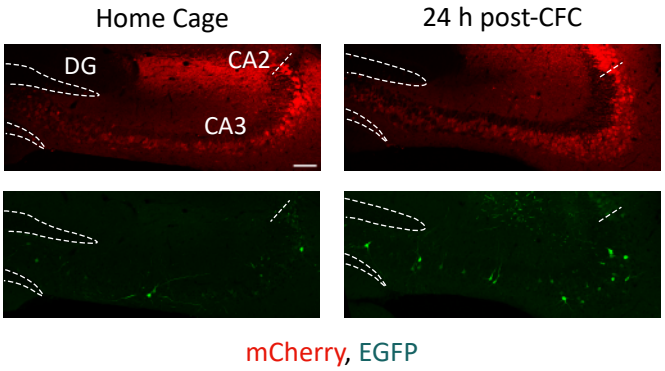

Figure S4

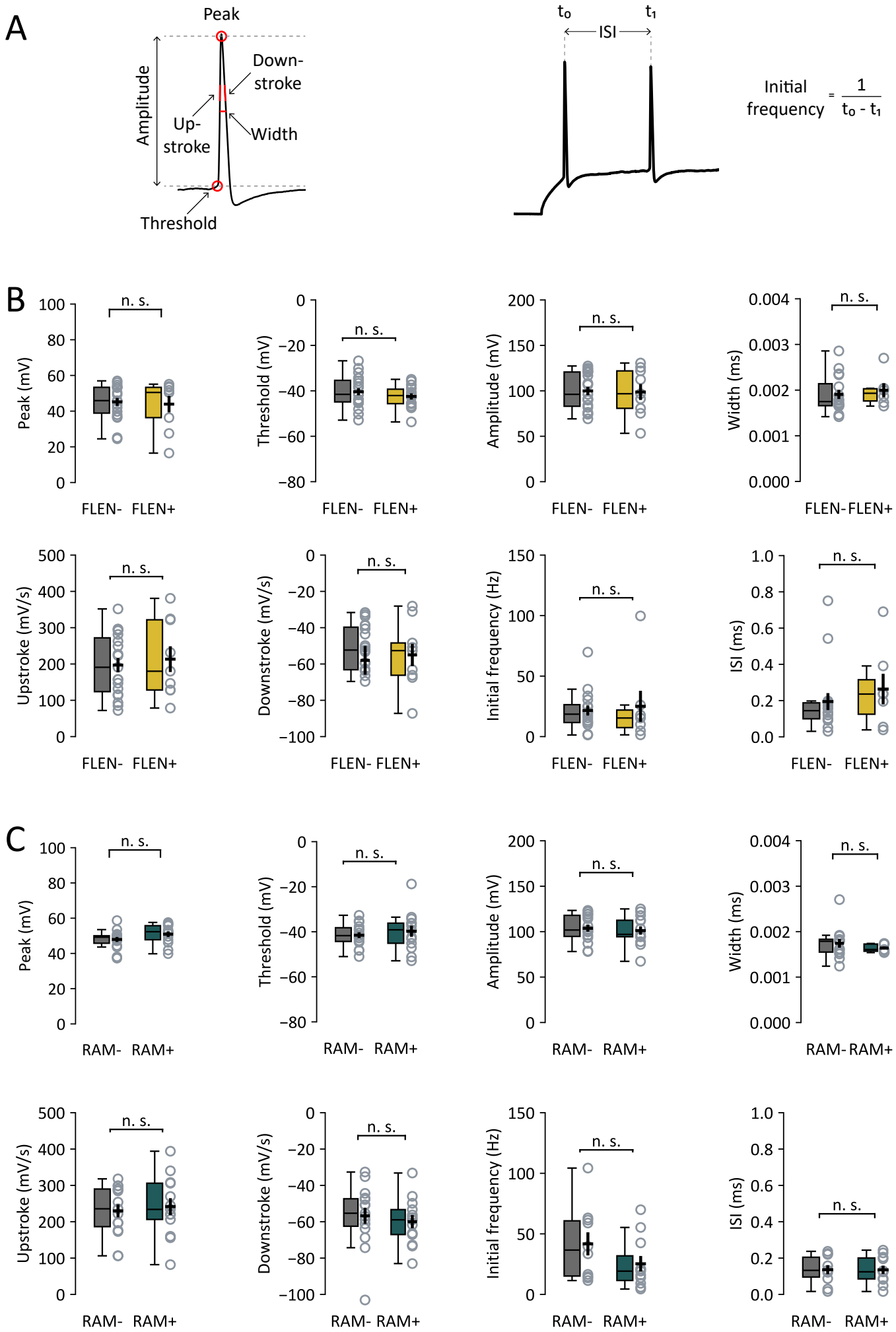
A
Peak
Amplitude
Down-stroke
Up-stroke
Width
Threshold
t₀
t₁
ISI
Initial frequency = 1 / (t₀ - t₁)
B
Peak (mV)
Threshold (mV)
Amplitude (mV)
Width (ms)
Upstroke (mV/s)
Downstroke (mV/s)
Initial frequency (Hz)
ISI (ms)
n. s.
FLEN-
FLEN+
C
RAM-
RAM+